ARTICLE

Dynamics of bound states of dihydrogen at Cu(I) and Cu(II) species coordinated near one and two zeolite framework aluminium atoms: A Combined Sorption, INS, IR and DFT study

P. A. Georgiev,*[a] N. Drenchev[b], K. I. Hadjiivanov[b], J. Ollivier[c], T. Unruh[d], and A. Albinati[e]

Ambient conditions sorption isotherms of dihydrogen in a series of various levels of Cu-exchanged ZSM-5 zeolites, with two different Si/Al ratios, namely 11.5 and 25, show the presence of different amount of Cu centres able to strongly bind H_2. Although the isosteric heats of adsorption derived from these isotherms are rather similar, of the order of 30 kJ/mol H_2, Inelastic Neutron Scattering (INS) of adsorbed dihydrogen and Fourier-Transformed Infra-Red (FTIR) spectroscopy measurements of adsorbed CO and NO reveal that copper is encountered in two oxidation states. At least two types of Cu(I) ions are clearly detected as well as some heterogeneity of the Cu(II) species. The number of these Cu species is different in the two investigated ZSM-5 materials and depends on the Cu exchange level. With the aid of DFT model cluster calculations we find that under different coordination environments, determined by the Al distribution, both mono- and divalent Cu ions could bind H_2 with a different strength. Unprecedentedly, we found that Cu-ions compensating two Al atoms, i.e. formally Cu(II) species, relatively far apart from each other, may behave very similarly to the monovalent Cu-species or alternatively viewed – as Cu(I) species that compensate for two framework Al-atoms. Such Cu-species also form stable η^2 dihydrogen complexes.

Introduction

Due to their ability to stabilise metal ions in highly reactive electronic states, with low coordination number, within an open for various guest molecules pore structure, ZSM-5 zeolites continue to attract an intense scientific and industrial interest. Perhaps the most valuable merit of Cu-exchanged ZSM-5 is its high activity in reactions for NO_x control, such as direct decomposition of NO [1] and selective reduction of NO_x by hydrocarbons [2,3]. The catalytic properties of the Cu-ZSM-5 materials have been well established from a macroscopic point of view and the corresponding research work comprehensively reviewed [4]. One of the outputs is showing that the activity of the material depends on the Si/Al-ratio, the copper loading, and, to some extent, on the preparation conditions [4]. It has been suggested by early studies [5] that monovalent Cu ions are responsible for the observed high catalytic activity. The reducibility of the Cu ions in Cu-ZSM-5 in vacuum, H_2, and CO,

as well as the Cu(I)-ion sitting have been further investigated [6-8] by means of UV-vis photoluminescence and *in situ* NO Fourier-Transform Infra-Red (FTIR) spectroscopy. Two main types of Cu(I) species have been found [6-8], with concentration ratios depending on the Si/Al ratio and the Cu concentration correlating well to the observed catalytic activities. The Cu ion coordinated near a single Al-atom, presumably to two framework oxygen atoms only, has been suggested as an active site, in contrast to the second type of sites in which the Cu ion is coordinated to three framework oxygens, very likely in the vicinity of two Al-atoms [8]. The autoreduction process in which Cu(II) is reduced to Cu(I) by temperature treatment in vacuum as well as the Cu ion local coordination environment and activity have been further studied by X-ray spectroscopic techniques and *in situ* FTIR measurements of adsorbed NO and CO [9-14]. Thus, in highly siliceous samples e.g. Si/Al=25÷45, after vacuum activation at 673 K, more that 90% of the total Cu content has been found in a monovalent state in which the Cu(I) ion resides 2.00±0.03Å away from the nearby oxygen atom, with an average coordination number of 2.5±0.3 [9]. Under similar conditions, about 40% of the total Cu content has been reduced to Cu(I) for a Cu-ZSM-5 sample with Si/Al=14 [10]. Another study [12], concluded that for samples with higher Al content, Si/Al=11.9, 46% of the Cu ions are in the form of Cu(I) after evacuation at 673 K. The reduction process evidently continues with the increase of the temperature, reaching 56% at 773 K and 70% at 873 K [13]. For a very similar sample with Si/Al=11.9 the same group has reported an average coordination number of 2.8 and an average Cu-O distance of 1.98 Å [14]. The trend of increase of the Cu(I) coordination number and decrease of its

a. Condensed Matter Physics and Microelectronics Department, The University of Sofia, J. Bourchier 5, Sofia 1164, Bulgaria
b. bInstute of General and Inorganic Chemistry, Bulgarian Accademy of Sciences, G.Bonchev str, bld 11, Sofia 1113, Bulgaria
c. cInstitute Laue-Langevin, 6 rue Jules Horovitz, BP156, F-38042 Grenoble Cedex 9,Grenoble, France
d. Institute of Condensed Matter Physics, Friedrich-Alexander-Universität Erlangen, Nürnberg,Germany.
e. CNR - Istituto di Chimica dei Composti Organometallici (ICCOM)Sesto Fiorentino, Florence Italy and University of Milan, Milan, Italy, University of Milan, 19 Via C. Golgi, 20133 Milan, Italy.

fractional content with the increase of the Al-substitution is supported by other studies on Cu-exchanged mordenite material with Si/Al=5 [11]. In this case the coordination number varies from 4.1±0.4 for Cu(II) to 2.9±0.3 for Cu(I) after evacuation at 673K [11], with at least 30% of the Cu remaining in the divalent state. The above experimental observations [6-14] may be rationalised by assuming that various Cu coordination sites are associated with different aluminium tetrahedral site preferences. Following the notation of the non-equivalent Si(Al) crystallographic positions [15], and employing combined interatomic potential function for the periodic zeolite structure and *ab initio* quantum mechanical methods for the atoms defining the particular coordination site, Nachtigalová et al. [16] have evaluated the stability of Al substitution in each of the 12 possible non-equivalent tetrahedral positions (T-sites). More recently [20] the stability and energetic preference of formation of various combinations of framework Al-pairs has been computationally explored in a great detail. It has been experimentally established [21] that at low Cu loadings, e.g. below 1% wt, bare Cu(II) ions are abundant, compensating two framework Al-atoms. EXAFS data suggest the formation of oxygen bridged linear dinuclear Cu-species at higher loadings [21]. It has been computationally shown [22] that at high Cu-loadings even trinuclear Cu-species may be thermodynamically rather stable. This seems to have been again corroborated experimentally [21]. However, EXAFS studies on the distribution and dynamical structure of Cu-species in the Chabazite structure SSZ-13 demonstrate that equally good fits may be obtained by considering neighbouring Al(Si) tetrahedral atoms [23]. Yet again, in Cu − exchanged SSZ-13, similarly to the findings for Cu-exchanged ZSM-5 [21], EXAFS experiments [24] suggest possible formation of oxygen bridged binuclear Cu-species only at high Cu loadings, e.g. 1.2 % wt Cu and only monomeric species for medium loadings of 0.5% wt Cu.

The interest in the Cu-exchanged ZSM-5 zeolites, particularly for dihydrogen binding and storage, has been recently revived by reports on some extraordinarily strong interaction with dihydrogen [25, 26] raising a fundamental interest in utilising this type of binding interactions as a prototype of solid state hydrogen storage media. In a previous work [27] we have confirmed that the hydrogen molecule is chemically bound to a low coordination number Cu-centre and forms a nonclassical η^2-hydride, a.k.a. Kubas's complex [28]. The observed spectroscopic features [27], a sharp peak centred at about 0.8 cm^{-1} and much broader bands at 1.4 and 1.7 cm^{-1}, appearing at higher loadings, were interpreted in terms of adsorption on Cu ions in various coordination environments, with only the lowest energy peak unambiguously modelled as an η^2-Cu(I) complex coordinated at two framework oxygen atoms. Note the erroneous units given in the caption of Figure 1 of [27] – the correct units on the energy axis are cm^{-1}. The broad bands at around 1.4 and 1.7 cm^{-1} were tentatively assigned to dihydrogen on Cu(I) ions sitting in a very diverse coordination environment. Multiple dihydrogen binding at a single Cu(I) centre was rejected by the simulations [27]. Consequently, we have also measured and reported [29] dihydrogen adsorption isotherms at ambient temperatures and extracted the

corresponding isosteric heats of adsorption in a broad concentration range covering about 40% of the isolated Cu-ions. For these we obtained isosteric heats starting at 80 kJ/mol H$_2$ for the lowest concentrations, flattening out at e.g. 50-60 kJ/mol and then continuously dropping down to about 40 kJ/mol for the highest accessed loading corresponding to 0.4 H$_2$/Cu. More recently, the possibility of storing hydrogen via chemical adsorption has been further explored in Cu(I) exchanged ZSM-5, SSZ-13 and SSZ-39 using only Cu(I) source such as CuCl in acetonitrile solution [30, 31], thus achieving high loading of monovalent Cu-species, again assuming that isolated Cu(I) species are responsible for the extraordinarily strong binding of the adsorbed hydrogen. The strong binding was explored by other authors [32] aiming at quantum separation of hydrogen isotopes, owing to the large enough difference in the vibrational energies of the isotopes, a factor of 2 for H$_2$ and D$_2$ at the strong-binding sites.

In the present work, we extend our studies on Cu-exchanged ZSM-5 zeolites focussing on low exchange levels, in different Si-to-Al materials, aiming to shed more light on the details of dihydrogen binding and metal ion activities at isolated Cu-ions compensating either a single or two Al framework atoms at various distances from each other, positioned in a single or different zeolite rings. The dynamics of dihydrogen bound at such Cu species, as we will show not necessarily of oxidation state (I), is observed by high resolution INS and is able to explain the previously unassigned [27] peculiar broad bands in the corresponding low temperature INS spectra.

Experimental

Materials and Synthetic procedures

The ammonium forms of ZSM-5 zeolites with Si/Al ratios of 11.5 and 25 (CBV2314G and CBV5524G), purchased from Zeolyst, USA, were converted into the corresponding protonated forms by calcinations at 823 K for about 2 hours. Copper ion exchange was performed in aqueous solutions of copper acetate with concentrations between 0.002 and 0.023 M in a single step process. The exchanged materials were filtered out, washed and dried at 393 K for about 16 hours. The total copper content in each sample was determined by Atom Absorption Spectroscopy (AAS).

Research grade dihydrogen gas (99.9995%) was used throughout all measurements. Carbon monoxide (> 99.5 % purity) was supplied by Merck. Before adsorption, the CO gas was passed through a liquid nitrogen trap. Nitrogen monoxide was provided by Messer Griesheim GmbH, and had a purity of > 99.0%. Prior to the adsorption procedure the NO gas was purified by fraction distillation. text of the article should appear here with headings as appropriate.

Techniques

Dihydrogen adsorption isotherms were measured with a Sieverts type volumetric gas handling rig. The samples were placed in a stainless steel reactor for activation and isotherm measurement. Details of this experimental set up have previously been given [27, 29]. The activation and isotherm measurement procedures reported

before [29] were followed here as well; with the only difference that now we used larger samples of the order of 10 g each. Isotherms at three different temperatures were measured for each sample in order to determine the corresponding isosteric heats of adsorption. Additionally, at the same three temperatures, dihydrogen adsorption isotherms of the two 'blank' H-ZSM5 materials, CBV2314G and CBV5524G, were also measured. Their fourth power polynomial interpolants were consequently subtracted from the isotherms of their Cu-containing counterparts in order to obtain isotherms corresponding to adsorption on Cu ions only, as shown in the SI material.

FTIR investigations were carried out using a Nicolet Avatar 360 spectrometer, at a spectral resolution of 2 cm^{-1}, by accumulating 64 scans per spectrum. Self-supporting pellets ($\approx$ 10 mg cm^{-2}) were prepared by pressing the sample at 10^4 kPa and were always treated in situ in the purpose-built IR cell. The latter was connected to a vacuum apparatus with a residual pressure of about 10^{-3} Pa. Prior to the adsorption measurements, the sample was activated by heating for 1 h at 723 K under oxygen followed by evacuation for 1 h at the same temperature.

INS spectra of dihydrogen adsorbed in large batches of the same samples were collected on the time-of-flight direct geometry chopper spectrometers IN5 [33] and TOF TOF [34]. Prior to the INS experiments each Cu-ZSM5 sample was activated in a stainless steel container at up to 823K, in a dynamic vacuum of the order of 10^{-6} Torr, then transferred to an aluminium scattering cell attached to a centre stick equipped with gas capillaries. The transfer procedures were accomplished in a He-filled glove bag. In situ dihydrogen dosing was performed with the same gas handling rig as for the adsorption isotherm measurements. After recording a blank spectrum for each sample i.e. with no dihydrogen, at 4K, using neutrons with wavelengths of 2 Å and 7 Å, calibrated amounts of dihydrogen gas were introduced into the scattering cells at around 100 K. After each pressure equilibration step, the temperature was decreased again to 4 K and the corresponding spectra were measured using the same neutron wavelengths. One reference INS spectrum of 20 cc (STP) H$_2$ per gram, adsorbed in a H-ZSM-5 sample (Si/Al=25), was also measured at 4K.

Computational details

Dihydrogen rotational dynamics and adsorption site strengths were studied using clusters cut out from the original MFI structure, consisting of 23 Si(Al)O$_4$ tetrahedra, closely resembling Cu-sites at the intersection of the straight and sinusoidal channels for both Cu(I) and Cu(II) ions. The results were checked against similar accuracy periodic model DFT calculations based on the Chabazite structure as a test bed. The multiprocessor version of Gaussian 09 computational package [35] was used for the cluster simulations while the Abinit package, version 8, was employed for the periodic model studies. Full details of the computational setups are provided in the Supporting Information.

Results and discussion

The following nomenclature was adopted in order to label the investigated samples: the approximate Si-to-Al ratio in each sample was abbreviated as SAX, X=Si/Al ratio, i.e. SA12 and SA25 for our two

bare zeolite materials; the Cu-to-Al exchange level is given shortly as CuX, X=Cu/Al ratio. Thus, where the Cu/Al ratio, as determined by Atomic Absorption Spectroscopy (AAS) is 0.25, the corresponding part of the sample's label is Cu0.25. The full label of a sample with Si/Al of 25 and Cu/Al=0.25 thus becomes SA25Cu0.25. Table 1 and 2 summarise some physical and chemical properties of our samples with the two different Si/Al ratios of 11.5 and 25, accordingly.

4.1. Volumetric dihydrogen adsorption

The isosteric heats of dihydrogen adsorption at low coverage in the H-form of the two parent ZSM-5 materials are shown in Fig. 1. The corresponding adsorption isotherms measured at the three experimental temperatures namely 273, 294, and 314 K, are given in the Supporting Information along with the isotherms of each of the two zeolites exchanged with different amount of copper ions.
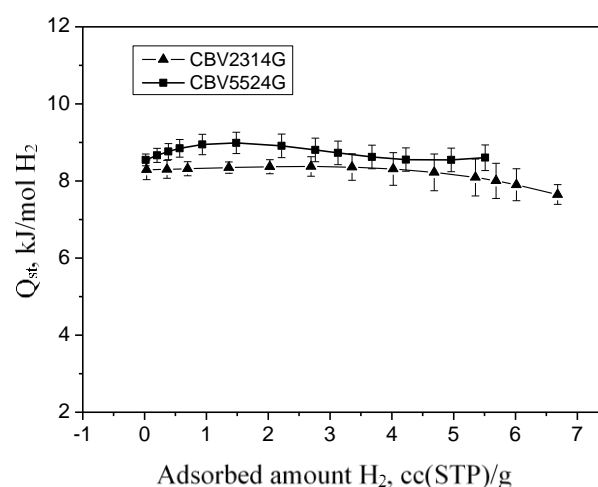

Figure 1. Isosteric heats of adsorption of the two 'blank' H-ZSM-5 zeolites as functions of the dihydrogen loading, measured in the interval 273 – 314 K.
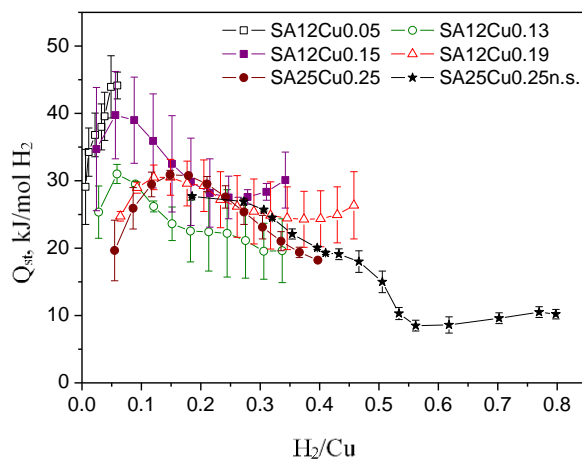

Figure 2. Isosteric heats of adsorption of Cu-exchanged ZSM-5 samples as indicated in the figure legend, measured in the temperature interval 273 – 314 K. The Q$_{st}$ curve of the SA25Cu0.25 sample is also reported (black solid stars) from the corresponding not subtracted isotherms.

Table 1. Observed properties of the Cu-exchanged ZSM material CBV5524G referred to as SA25. R_1 is the maximum integral intensity ratio at saturation of the IR lines of Cu(I)(CO)$_3$ and Cu(I)(CO)$_2$ and R_2 – for Cu(I)(CO)$_3$:Cu(I)CO. Q_{st} is the measured isosteric heat of H$_2$ adsorption and ω_t – the observed by INS H$_2$ rotational tunnelling frequencies.

Sample	Cu[COOCH$_3$]$_2$ mol. conc.	Cu, %wt	Cu(I)/Cu(II) NO*	R$_1$, R$_2$	H$_2$/Cu	Q$_{st}$, kJ/mol H$_2$	ω_t, cm^{-1}
SA25Cu0.00	n.a.	0.0	n.a.	n.a.	n.a.	9.1±0.2	n.a.
SA25Cu0.19	0.004	0.77	0.72	0.44 0.37	-	-	±0.8
SA25Cu0.25	0.006	1.01	3.5	0.33 0.29	0.73	25±5	±0.8, ±1.4
SA25Cu1†	0.01	3.43	-	- -	0.54	40-74	±0.8, ±1.4

*The ratio between the IR lines of NO adsorbed on Cu(I) and Cu(II). †From references 27 and 29

Table 2. Observed properties of the Cu-exchanged CBV2314G sample referred to as SA12.

Sample	Cu[COOCH$_3$]$_2$ mol. conc.	Cu, %wt	Cu(I)/Cu(II) NO*	R$_1$, R$_2$	H$_2$/Cu	Q$_{st}$, kJ/mol H$_2$	ω_t, cm^{-1}
SA12Cu0.00	n.a.	0.0	n.a.	n.a.	n.a.	8.3±0.2	n.a.
SA12Cu0.05	0.002	0.38	-	-	0.09	37±5	-
SA12Cu0.13	0.005	1.01	-	-	0.47	24±4	-
SA12Cu0.15	0.006	1.16	0.56	0.42 0.38	0.45	32±4	**0÷4**
SA12Cu0.19	0.023	1.55	0.63	0.71 0.51	0.61	28±2	±1.4

The average isosteric heats of adsorption of the two H-ZSM-5 samples are almost equal within their estimated errors and may be compared to the 6.0 kJ/mol H$_2$ heats of adsorption of dihydrogen in silicalite [36] as well as in Na- and K-exchanged ZSM-5 [37] namely 10.3 and 9.1 kJ/mol H$_2$. Thus, there is about 50% increase in the adsorption heat on going from the neutral pure silica to the protonated Al-containing zeolite form. Further, as seen in Fig. 2, the replacement of the acidic protons by Cu ions, most likely both di- and monovalent as will be shown later, leads to a three to four-fold increase in the corresponding isosteric heat. The average all data points on each curve in Fig. 2 is reported in the Q$_{st}$ columns in Tables 1 and 2 accordingly.

It may also be noted that for the SA25Cu0.25 samples, for which we have also shown the Q$_{st}$ curve, resulting from H-ZSM-5 unsubtracted isotherms, there is a clear and significant drop of the adsorption heat down to about 10 kJ/mol H$_2$ at about 0.5 H$_2$/Cu that is very close to the values for the non-exchanged zeolite materials. This indicates that at these H$_2$ concentrations most of the dihydrogen is adsorbed at the weaker Cu(II) sites and the rest of the zeolite framework.

In all the presently investigated samples, the measured isosteric heat of adsorption at the lowest loadings is on average lower than that determined for H$_2$ in the over-exchanged Cu-ZSM-5 material [29]. The experimental Q$_{st}$ values are, however, similar near the middle of the accessed concentration range where the adsorption heat of H$_2$ in the over-exchanged material [29] settles near 40 kJ/mol, before dropping down to about 30 kJ/mol at loadings of about 0.5 H$_2$/Cu. These observations may suggest that in the over-exchanged material some additional and stronger adsorption sites must be present.

FTIR characterisation
IR spectroscopy of probe molecules e.g. CO and NO was used for an additional and independent identification of the different copper species.

CO adsorption
FTIR spectroscopy of adsorbed CO is a powerful frequently used technique for the characterization of Cu(I) species. The Cu(I)–CO bond is relatively strong due to the synergism between its σ- and π-components [41]. In addition, the formation of π-back bonding

enhances the C–O extinction coefficient which allows detection of relatively small amounts of Cu(I) sites.

It has been reported that Cu(I)–CO species in Cu–ZSM-5 are characterized by an unusual high frequency [38-41] (2158 cm^{-1}) as compared to carbonyls formed with oxide-supported copper [41-43] and this has been attributed to the enhanced σ-component of the Cu(I)–CO bond [41]. It has also been found that, at room temperature and in the presence of CO in the gas phase, the monocarbonyls tend to be converted to dicarbonyl species [38-42]:

$$Cu(I)–CO + CO \leftrightarrow Cu(I)(CO)_2 \qquad (1)$$
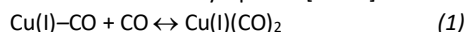
These dicarbonyls manifest themselves by IR features at ν_s(CO) at 2178 cm^{-1} and ν_{as}(CO) at 2151 cm^{-1}, symmetric and antisymmetric intramolecular C-O stretches accordingly. Zecchina et al.[39] reported that at low temperature conversion of di- to tricarbonyl species also takes place:

$$Cu(I)(CO)_2 + CO \leftrightarrow Cu(I)(CO)_3 \qquad (2)$$
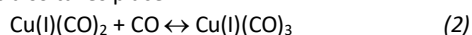
It has been concluded that the tricarbonyls are characterised by two bands at 2191 and 2167 cm^{-1}. In addition, a band at 2137 cm^{-1}, coinciding in position with the band characterizing physisorbed CO, has been proposed to be due to the same complex [39]. The authors noted, however, this was a tentative assignment and that not all dicarbonyl species could be converted into tricarbonyls.

There is currently no consensus in the literature about the possibility of detection of Cu(II) sites in zeolites by CO [37]. In any case, the Cu(II)–CO bond is much weaker compared to the Cu(I)-CO bond. For that reason, Cu(II) sites may be detected using CO only at low temperatures.

Contrary to CO, NO forms relatively strong complexes with Cu(II) ions [46] while the Cu(I)-NO bond is rather weak and these complexes are formed at lower temperatures [47]. However, highly coordinatively unsaturated Cu(I) cations in zeolites can form nitrosyls even at room temperatures while at low temperature these species are converted to dinitrosyls [48].

In this work we initially exploited the capabilities of IR spectroscopy of adsorbed CO to characterize the Cu(I) ions formed during autoreduction of Cu(II) on several Cu-ZSM-5 zeolites differing in copper loading and Si : Al ratio. Data on the fractions of Cu(I) sites able to form tricarbonyls were obtained. Further, NO was used as a molecular probe to obtain information on the ratio between Cu(II) and Cu(I) species.

Four samples were selected for the FTIR studies: SA25Cu0.19, SA25Cu0.25, SA12Cu0.15 and SA12Cu0.19. The background IR spectra of these activated samples, in the OH region, are presented in Fig. 3. The spectrum of SA25Cu0.19 contains three main bands at 3744, 3655 and 3612 cm^{-1} (Fig. 3, spectrum a). A shoulder around 3726 cm^{-1} is also visible. In addition, a broad absorbance, centred on 3500 cm^{-1}, can be distinguished too.

The band at 3744 cm^{-1} is known to arise from external silanol groups and that at 3726 cm^{-1} to internal silanols [49]. The band at 3612 cm^{-1} corresponds to zeolite acidic hydroxyls and indicates an incomplete ion-exchange which is consistent with the low Cu:Al ratio (see Table 1). In any case, the band is reduced in intensity as compared to the parent zeolite. The band at 3665 cm^{-1} is associated with Al-OH groups and evidences the existence of EFAL species [49]. Finally, the broad band around 3500 cm^{-1} is due to H-bonded hydroxyls. The spectrum of SA25Cu0.25 shows the same features (Fig. 3, spectrum b). In this case, however, the band due to bridged hydroxyls is less intense,

which indicates a higher exchange degree and is consistent with the higher copper concentration in the sample. The spectrum of SA12Cu0.15 is noisier (Fig. 3, spectrum c). This is due to the fact that the transmission of the sample in the region is rather low, which is attributed to a larger particle size and enhanced light scattering. In any case, the same features as with samples 1 and 2 can be distinguished. As expected, the spectrum of SA12Cu0.19 (based on the same parent zeolite) is also noisy. In this case, the OH bands are poorly resolved and less intense. This indicates that some copper species have reacted not only with the acidic hydroxyls, but with the other OH groups.
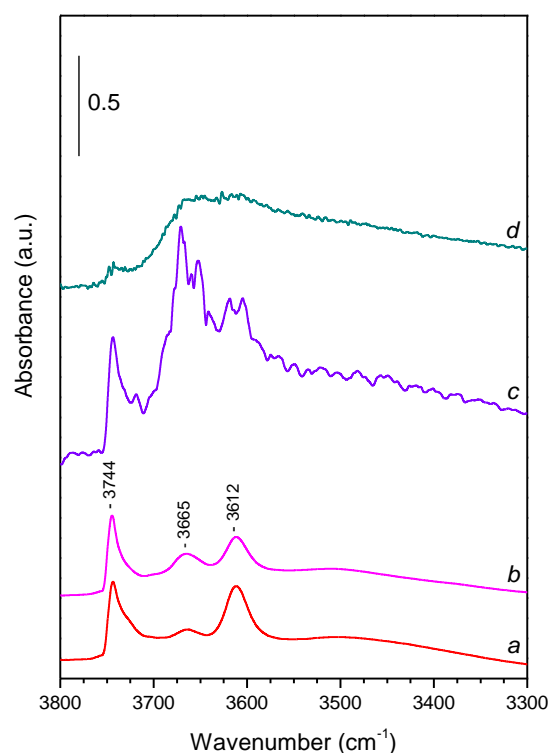

Figure 3. FTIR spectra of samples SA25Cu0.19 (a), SA25Cu0.25 (b), SA12Cu0.15 (c) and SA12Cu0.19 (d) in the OH region.

Adsorption of CO on SA25Cu0.19

Carbonyl species in this material showed rather exciting behaviour and their characterisation was published in a separate article [50]. In summary, these results confirmed the formation of Cu(I)–CO species on Cu-ZSM-5 that may be converted into dicarbonyls, and part of them, even to tricarbonyls. Some Cu(II) species were also detected at low temperature by a carbonyl band at 2194 cm^{-1}.

In order to obtain information on the conversion of di- to tricarbonyls, the intensities of the characteristic bands at 2191 and 2151 cm^{-1} were analized as a function of the coverage. It was found that about 45 % of the Cu(I) sites in this sample that are in cationic positions are able to coordinate up to three CO molecules, while the

remaining 55 % of the sites can form only dicarbonyls [50] The results of these studies is now reflected in the corresponding lines integral intensity ratios R1 and R2 in Tables 1 and 2. In addition to the carbonyl bands associated with copper, there were bands due to CO-OH interaction: CO polarized by the zeolite acidic hydroxyls at 2175 cm^{-1}; CO interacting with aluminol groups, at 2170 cm^{-1}, and CO affected by the silanol groups – around 2155 cm^{-1}.

Comparison of CO adsorption features on all samples

The carbonyl spectra detected after CO adsorption on SA25Cu0.25 are similar to those already described with SA25Cu0.19 (Fig. 4, spectrum b). The most important differences are:

- The band at 2175 cm^{-1} is less intense, which is consistent with the lower concentration of bridged hydroxyls on the sample.

- The band at 2170 cm^{-1} appears with enhanced intensity in agreement with the more important concentration of Al-OH species in this sample.

- All bands assigned to copper carbonyls and polycarbonyls are more intense in line with the higher concentration of copper.
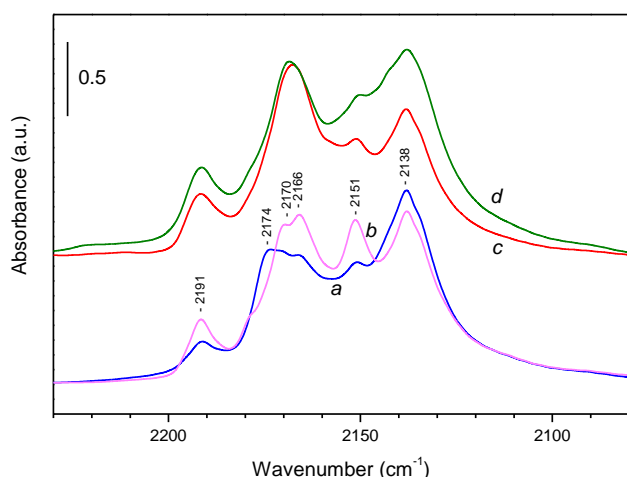
Figure 4. FTIR spectra of CO (50 Pa) equilibrium pressure) adsorbed at 100 K on SA25Cu0.19 (a), SA25Cu0.25 (b), SA12Cu0.15 (c) and SA12Cu0.19 (d). The spectra are background corrected.

In agreement with the established highest copper content in SA12Cu0.19, the carbonyl spectra, registered after CO adsorption here, show the highest intensity of the band due to tricarbonyls (Fig. 4, spectrum d). In addition, the highest level of conversion from di- to tricarbonyls was detected for this sample. Some amount of EFAL Lewis acid sites were also detected by an Al^{3+}-CO band at 2220 cm^{-1}. Interestingly, the FWHM of the 2158 cm^{-1} monocarbonyl band with the two SA25Cu samples is 8 cm^{-1} while with the samples SA12Cu, 12 cm^{-1}. This suggests a more homogeneous copper distribution in the samples SA25Cu.

Adsorption of NO

The IR spectra of NO (1.6 kPa equilibrium pressure) adsorbed on the samples are shown on Fig. 5.
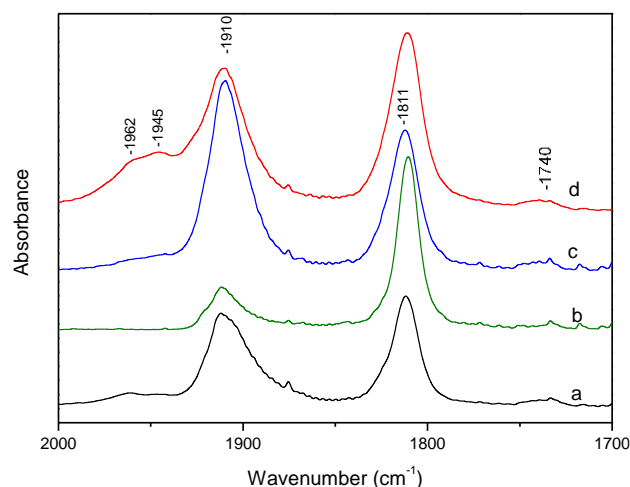
Figure 5. FTIR spectra of NO adsorbed at room temperature on SA25Cu0.19 (a), SA25Cu0.25 (b), SA12Cu0.15 (c), and SA12Cu0.19 (d). The spectra are background corrected.

The bands above 1850 cm^{-1} are usually assigned to Cu(II)-NO species while the bands below this frequency originate from nitrosyls of Cu(I) [46]. The band at 1910 cm^{-1} is assigned to NO adsorbed on isolated Cu(II) sites. Clearly, all samples contain significant amount of isolated Cu(II) sites. A careful analysis of the related NO spectra reveals that these sites have slightly different coordination environments. The band at 1811 cm^{-1} is typical of Cu(I)-NO species in Cu-ZSM-5 [48]. A negligible fraction of these species are converted into dinitrosyls at the conditions used, being evidenced by the weak relatively broad band at around 1740 cm^{-1}. A shoulder of the main band (1811 cm^{-1}) appears at around 1827 cm^{-1}. Note that, in agreement with the CO adsorption results, the Cu(I)-NO bands with the SA12Cu samples are broader thus again indicating a larger inhomogeneity of the Cu(I) sites in this higher Al-content material.

In situ Inelastic Neutron Scattering of adsorbed dihydrogen

Owing to its large neutron scattering cross section, about an order of magnitude larger than that of other chemical substances, as well as the relatively large rotational constant, B=59 cm^{-1}, dihydrogen is a very sensitive and convenient probe for studying diverse adsorption sites, their strengths, and spatial shapes. Such data provides a unique detailed microscopical description of porous-materials internal surfaces and their heterogeneity. This is achieved by observing the spectrum of lowest energy rotational states of the adsorbed molecules. In comparison to that in the free state, this spectrum is strongly modified by the local adsorption potential, depending on each site size, shape, and the local interactions strengths. In the rotationally free state, at low temperatures, and in thermodynamic equilibrium all molecules are in the spherically symmetric singlet state J=0. Being composed of half-spin particles, dihydrogen obeys Fermi-Dirac statistics. In order to preserve the required antisymmetric character of the total molecular wavefunction, with respect to the two nuclei interchange, neutron scattering processes

leading to rotational excitations to the triply degenerate spatially antisymmetric J=1 state (as well as any other transition between even and odd J states) is necessarily accompanied by a nuclear spin flip. The intensities of such transitions are proportional to the very large incoherent scattering cross section of hydrogen. The transition to the first excited state in the gas phase, is expected at about 119 cm^{-1}. In physisorption systems such as Grafoil the first rotational transition of the adsorbed dihydrogen, at concentrations corresponding to the commensurate $\sqrt{3}$ phase, has been observed at 117 cm^{-1} as a single sharp line [51]. On the contrary, the same feature appears split into a doublet and a singlet for H_2 adsorbed in Single-Wall Carbon Nanotubes [52] while a complex broad spectrum, extending between 80 and 140 cm^{-1}, has been observed for dihydrogen adsorbed in microporous activated carbon [51]. In Metal-Organic Framework (MOF) compounds with unsaturated metal sites such as HKUST-1 [53], containing Cu(II) centers coordinated to four oxygen atoms in a planar arrangement, the corresponding rotational component has been found at 72 cm^{-1} [54] and 100 cm^{-1} [55]. In CPO-27-M, (M =Mg^{2+}, Ni^{2+}, and Co^{2+}) a material with high density of the metal centres, in a square pyramidal coordination, the lowest excited H_2 rotational state has been observed between 52 and 60 cm^{-1} [56] for H_2 adsorbed only at the metal centre. For this set of equivalent topology metal-ion sorption sites, with similar coordination environments, the binding energy follows a relatively simple monotonic trend, with the position of the centre of the gravity of the corresponding rotational transitions [55, 56], which could serve as a miscroscopic indicator of the relative adsorptive site strengths. However, in general the interpretation of the data is more complicated due to the influence of steric interactions, for instance with host structural fragments, shaping the adsorption potential at a particular site. Thus, the most favourable sorption site in the [Zn(trz)(tftph)] MOF was identified, with aid of simulations, to be in the vicinity of a metal–coordinated H_2O molecule, an exposed fluorine atom, and a framework carboxylate oxygen. These coordination environments give rise to a rotational transition at 43.6 cm^{-1} and a measured adsorption heat of c.a. 8 kJ/mol [50]. In an yttrium-based Y-FTZB MOF (containing Y^{3+} open sites), on the other hand, the rotational transition has been observed at an even lower energy, e.g. 19.4 cm^{-1}, but with a similar isosteric heat of 9 kJ/mol H_2 [58]. This value is close to the lowest heats observed in the CPO-27-M materials [55, 56] too, but showing a much stronger rotational hindrance. In over-exchanged, predominantly Cu(I)-containing ZSM-5, due to the very strong interactions between the H_2 and the Cu(I) ions, an η^2-H_2 complex has been observed involving significant π back-bonding to the metal, [27] with the corresponding rotational line shifted even further down near 1 cm^{-1}, lowest to date with respect in any other porous material.

The above examples demonstrate the prospective of high resolution INS technique as a very sensitive and useful technique for probing the local adsorption site topology. However, the observation of the ground-to-first excited rotational transition of adsorbed dihydrogen, while representing a strong microscopic piece of information, cannot on its own serve as a definitive measure of the individual site adsorptive strength and therefore computational methods and/or complementary methods must be employed. The rotational spectra of dihydrogen, adsorbed in the under-exchanged Cu-ZSM-5 materials of this study, are shown in Fig. 6 a, b, c, and d. In all cases, features

previously observed in the Cu(I)-η^2-H_2 complex [27] are observed here too. Additionally, a useful differentiation of the signal is apparent too.
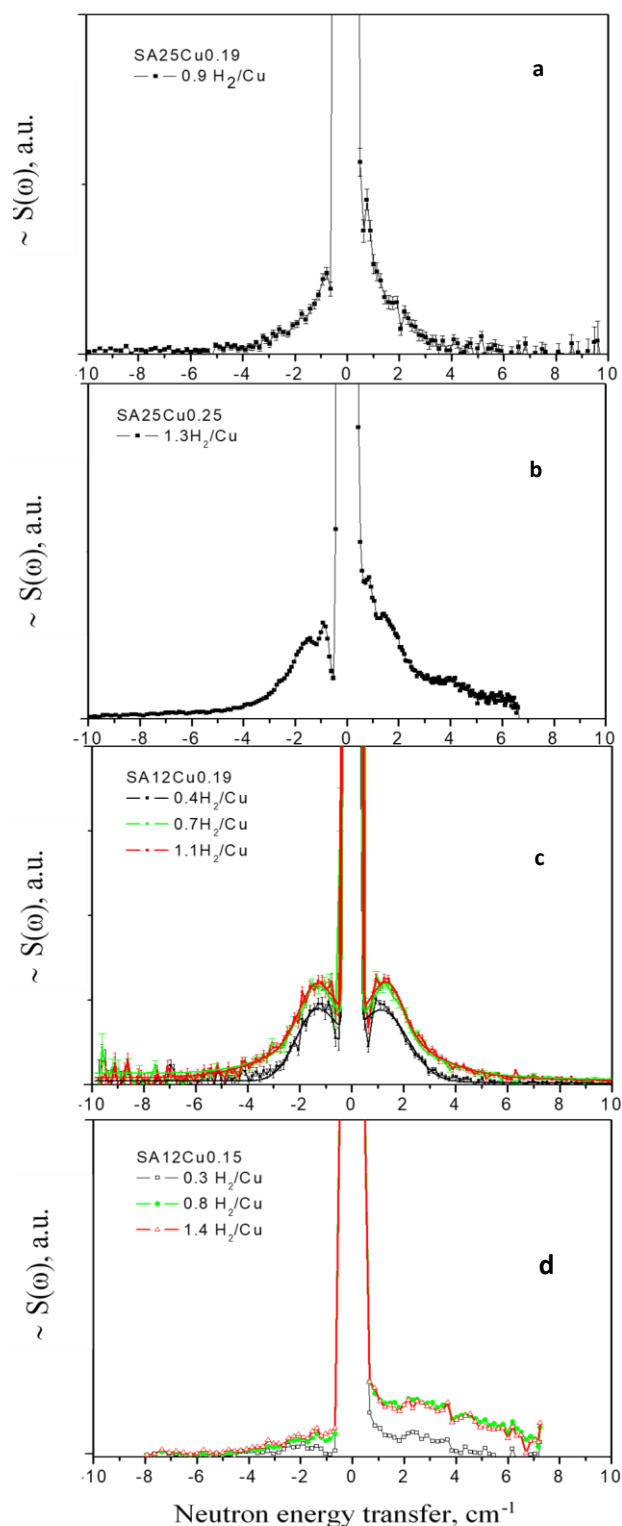

Figure 6. INS spectra of dihydrogen chemisorbed in: a) SA25Cu0.19, b) SA25Cu0.25, c) SA12Cu0.19, and d) SA12Cu0.15. Positive numbers along the energy axis correspond to neutron energy loss processes.

The dihydrogen spectra of samples SA25Cu0.19 and SA12Cu0.19 in Fig. 6, contain either the line at 0.88 cm^{-1} in the former spectrum or the broader band line at 1.49 − 1.79 cm^{-1} in the latter. Sample SA25Cu0.25 contains both features while SA12Cu0.15 shows only a rather broad continuum spanning a range up to 4-5 cm^{-1}. All features in this energy region are presumably due to H$_2$ chemisorbed on different Cu(I) species. In comparison to our previous study [27], here we have extended our measurements up to higher energy transfers allowing the observation of the rotational features of H$_2$ adsorbed both on the Cu(II) centres and on the zeolite skeleton, Fig. 7. The corresponding spectra are dominated by features at about 52, 60, 101 and 113 cm^{-1}. The first two are very close to the main spectral line of H$_2$ adsorbed at the Cu(II) sites in HKUST-1[54] and can therefore be rationalised in terms of H$_2$ adsorbed on different Cu(II) species which have not been reduced to Cu(I) during the high temperature vacuum treatment applied prior to the INS measurements. Bands, at 101 and 113 cm-1, could then be assigned to dihydrogen trapped in the ZSM-5 voids, whose rotational motion is weakly hindered mostly by the electrostatic potential of the ZSM-5 skeleton [59] and/or adsorbed on acidic protons. This scenario is suggested by subsequent measurements of dihydrogen adsorbed in H-ZSM-5 with Si-to-Al ratio of 25 showing H2 rotational peaks only at 99 and 116 cm-1, Fig. S5.
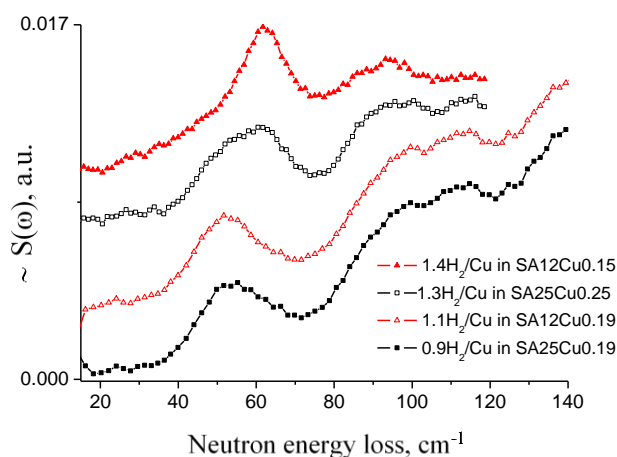

Figure 7. INS spectra of dihydrogen physisorbed to Cu(II) ions and acidic protons taken from the samples at higher dihydrogen loadings as indicated in the figure legend.

DFT calculations on model clusters and periodic structures

To check the above INS assignments and identify the different Cu species present in our samples, we compare the computed H$_2$ rotational tunnelling frequencies obtained from DFT calculations to the experimental features shown in Figures 8a-d and 9a-c with corresponding frequencies listed in Tables 1 and 2, respectively. .

Cluster models of the ZSM-5 MFI structure

The results from our cluster based calculations are presented n Tables 3 and 4. All rotational frequencies in Tables 3 and S2 were computed numerically, following the procedure as described in [27,

46], assuming a 1D rigid rotor model, using the zeolitic model clusters shown in Fig. 8. In Table 4 we present the NBO formal charges of the Cu atoms in different fragments, with and without adsorbed H$_2$, along with the corresponding Natural Atomic Orbital (NAO) configuration and the electronic population in the bonding and antibonding H$_2$ orbitals. The model structures, used in the calculations, were chosen so as to reconstruct in a simple and efficient way the positions and the corresponding coordination environment of the Cu atoms most easily accessible for guest species. The number of SiO$_4$ tetrahedrons in each model cluster allows for a realistic reproduction of the Si/Al ratios in the samples and the local electrostatic fields experienced by the adsorbed H$_2$. Inspection of Table 3 does confirm previous findings [25-28], based on small clusters, that monovalent Cu-species, represented here by the much larger clusters T23-AlT1-Cu(I), T23-AlT1HT4-Cu(I), and T23-AlT1HT7-Cu(I) bind dihydrogen strongly, resulting in a strongly hindered rotation [27]. The present larger structural clusters demonstrate again the dominant importance of the local coordination geometry of the Cu(I) species. Coordination to two framework oxygen atoms is associated with a more stable Cu(I)-H$_2$ complex, with a substantially stronger rotational hindrance of the H$_2$ ligand as compared to the four O-atom coordinated Cu(I)-ions for which both the binding energy and the barrier to rotation are reduced by factors of nearly 2 and 8, respectively. We recall that from a theoretical point of view, the dihydrogen rotational transition largely depends on the mode of binding at the metal centre and in particular to the electronic state of the metal ion, its coordination state, as well as the electrostatic and steric interactions with neighbouring framework fragments. Orbital interactions, leading to electron charge transfers and redistribution, are known to be essential in the η^2 metal-dihydrogen complexes [24] and this is intact with our results in Tables 3 and 4. The dispersive interactions, totalling to only about 10% of the binding energy, are expected to be rather isotropic, hence not significantly contributing to the bound-H$_2$ rotational barrier, and consequently have negligible effect on the rotational dynamics. The computed Cu-H$_2$ distances agree well to those previously observed in various 3d metal-dihydrogen complexes [28]. Notably, at coordinatively unsaturated Cu(II) species, orbital interactions are totally absent and the observed Cu(II)-H$_2$ distances increase to 2.3-2.8 Å, with the dihydrogen ligand freely rotating in the plane parallel to the Cu(II) square coordination plane [54, 55]. According to the NBO analyses here, Table 4, the very low rotational barrier in 4O-coordinated Cu(I)-ions is because, in contrast to 2O-coordinated Cu(I), the two different Cu 3d-orbitals involved in the back bonding, both in the equilibrium and in the transition state, are now of very similar shape and at similar energies. Thus, both orbitals are equally able to donate electrons, with the same magnitude of the corresponding energetic effect leading to a rather isotropic rotational potential. Comparing the data in Tables 3 and 4, becomes clear that the height of the barrier to rotation indeed depends on the amount of the electron π-back donation from the Cu 3d orbital to the H$_2$ σ^* antibonding orbital. There is a direct dependence of the barrier height on the difference between the electron back bonding in the equilibrium state and that rotated by 90° (i.e. the rotational transition state).

Table 3. Cluster (Gaussian) model Cu-H_2 complex results. Data in brackets for the Cu-H distance, H-H distance, the rotational barrier, V_2, and the tunneling frequency, ω_t, correspond to relaxed Cu-H and H-H lengths in the transition state with H_2 rotated by 90 degrees with respect to the equilibrium state. The BSSE corrected binding energy, E_b, is given along with the BSSE correction in brackets.

Fragment	$d(Cu\text{-}H)$, Å	$d(H\text{-}H)$, Å	E_b, kJ mol^{-1}	V_2, kJ/mol	ω_t, cm^{-1}
T23-AlT1-Cu(I)	1.638(1.673)	0.805(0189)	70.8(9.8)	11.8(11.1)	0.55(0.80)
T23-AlT1HT4-Cu(I)	1.642(1.675)	0.805(0.788)	71.0(9.5)	12.3(11.6)	0.46(0.69)
T23-AlT1HAlT7-Cu(I)	1.707(1.709)	0.787(0.787)	39.9(10.7)	1.61(0.16)	26.8(49.3)
T23-AlT1AlT23Cu(II)	1.696(1.729)	0.792(0.781)	60.0(10.1)	7.39(6.88)	2.59(3.44)
T23-AlT1AlT4-Cu(II)	1.682(1.715)	0.795(0.783)	58.9(10.6)	8.53(7.91)	1.70(2.35)
T23-AlT1AlT7-Cu(II)	2.43	0.746	1.6	0.79	43.6

Table 4. Computed NBO charge, H_2 molecular orbitals population and the Natural Atomic Orbital configuration of the Cu-species. The lower line data for each cluster type corresponds to Cu-species with no adsorbed H_2.

Fragment	Cu-charge	H_2 σ, e$^-$	H_2 σ^*, e$^-$	NAO
T23-AlT1-Cu(I)	0.45	1.889	0.071	4S(0.25)3d(9.85)4p(0.17)
	0.51			4S(0.11)3d(9.95)4p(0.08)5p(0.01)
T23-AlT1HT4-Cu(I)	0.44	1.889	0.068	4S(0.25)3d(9.85)4p(0.17)
	0.51			
T23-AlT1HAlT7-Cu(I)	0.34	1.910	0.049	4S(0.20)3d(9.90)4p(0.26)4d(0.01)
	0.36			4S(0.13)3d(9.96)4p(0.17)4d(0.01)5p(0.01)
T23-AlT1AlT23Cu(II)	0.51	1.892	0.051	4S(0.25)3d(9.85)4p(0.17)
	0.65			4S(0.13)3d(9.77)4p(0.08)4d(0.01)5p(0.01)
T23-AlT1AlT4-Cu(II)	0.46	1.897	0.057	4S(0.24)3d(9.78)4p(0.17)
	0.63			4S(0.13)3d(9.75)4p(0.09)4d(0.01)5p(0.01)
T23-AlT1AlT7-Cu(II)	0.58	1.946	0.003	4S(0.25)3d(9.27)4p(0.36)4d(0.01)5p(0.01)
	0.63			4S(0.26)3d(9.27)4p(0.31)4d(0.01)

Moreover, as most of the M-H_2 bond strength depends on the H_2 to M σ-bond (not affecting the barrier to rotation due to its symmetry) there is only an indirect relationship between the positions of the observed rotational transitions and the measured isosteric heat of absorption. The back donation of electrons from the Cu $3d_\pi$ orbitals into the H_2 σ^* orbital, leads to the expected H-H bond weakening [28], causing the red shift the H-H vibrational frequency. According to the calculations, the T23-AlT1-Cu(I) cluster with a Cu(I) atoms coordinated to two framework oxygens is the most likely candidate as the origin of the sharp rotational line at about 0.8 cm^{-1}. Nearly identical result is obtained for the T23-AlT1HT4-Cu(I) cluster, Fig. 8 and Ref. [27]. Weaker binding and much lower rotational hindering is found for H_2 at the 4O-atom coordinated Cu(I) in the T23-AlT1HT7-Cu(I) for the reasons discussed above. However, our INS spectra do not indicate the presence of the latter types of structures. Three and four oxygen-coordinated Cu(I) species at defect sites in the Cu-MOF-74(CPO-27-Cu) structure were recently anticipated and investigated computationally, again showing a decreasing H_2 binding power with increasing of the Cu(I) coordination [45]. Strong interactions between Cu(II) and H_2 have not been reported yet. Known isosteric heats for the Cu(II)-H_2 complexes as well as IR red-shifts correspond to a physisorption regime, e.g. 5-7 kJ/mol and 60 cm^{-1}[45] in agreement with the observed INS lines, in the range 55 – 80 cm^{-1} [54, 58]. Our computational results, based on the T23-AlT1T4-Cu(II) cluster also suggest low binding energy, of the order of just a few kJ/mol H_2.
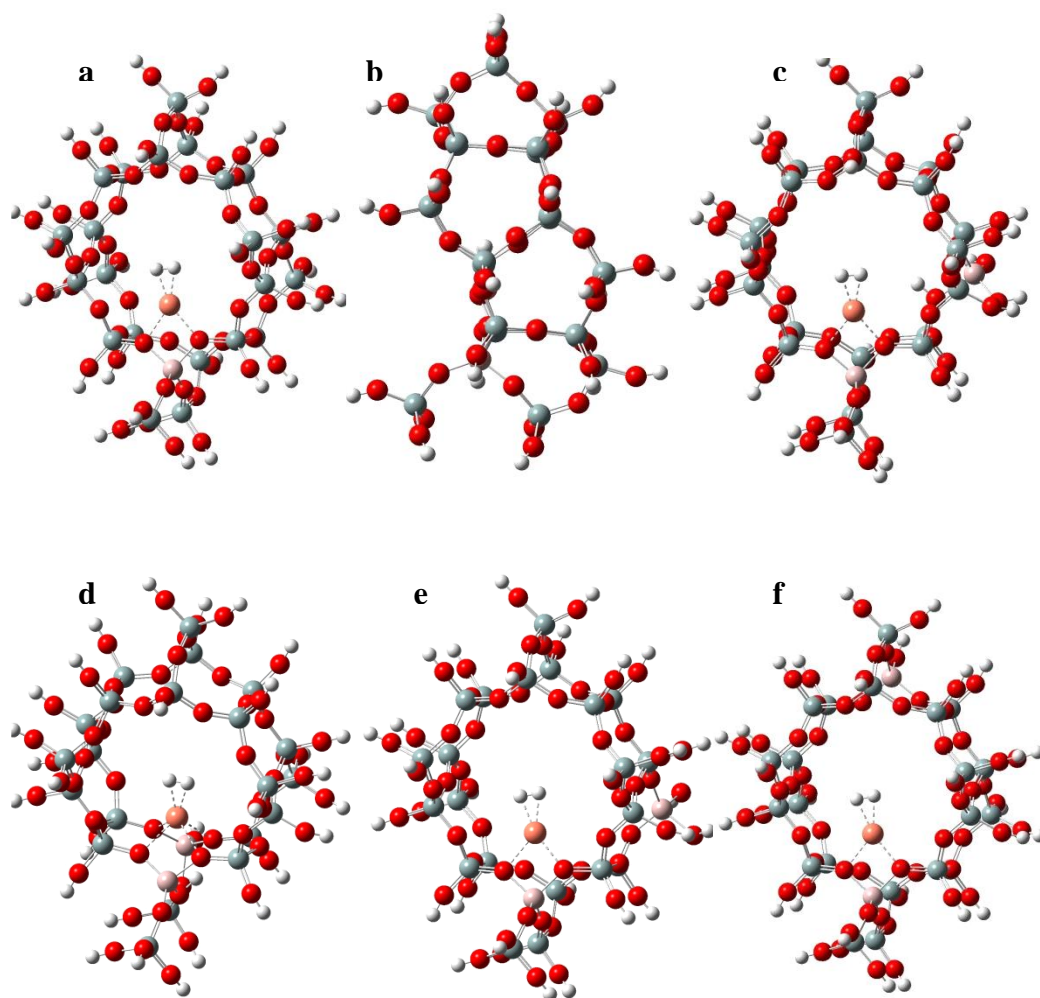
Figure 8. Zeolitic clusters with adsorbed H_2 in T23-AlT1-Cu(I) - front and side view in a) and b), in c) T23-AlT1HT4-Cu(I). T23-AlT1HAlT7Cu(I) is shown in d), followed by T23-AlT1AlT4-Cu(II) in e), and T23 on f)

NBO analyses for this adduct show practically no electron back donation, Table 5, and a typical Cu(II) chemistry, in terms of $3d_9$ electronic structure, large half-filled $3dz^2$ orbital, and relatively low reactivity. Correspondingly, the H_2 rotational tunnelling transition for this structure is predicted at about 44 cm^{-1}, Table 3, only marginally lower than that observed for the paddle-wheel Cu-sites in HKUST-1 [54]. Such 4O-coordinated Cu(II) ions may logically be expected as the most stable divalent species, that would hardly undergo autoreduction even at 873 K. We argue then that INS bands in the range 40-70 cm^{-1} originate from H_2 forming electrostatic adducts with Cu(II). Thanks to the larger size of the zeolitic clusters, we were additionally able to explore the extra framework Cu-ion electronic state and H_2 binding in configurations containing two Al atoms,

where one of the framework Al-atoms was moved further away from the other one: structures T23-AlT1AlT4-Cu(II) and T23-AlT1AlT23Cu(II). As seen in Fig. 8 **e** and **f**, the Cu atoms in such structures appear coordinated to only 2 oxygen atoms and their formal oxidation state, Table 4, formally is +1, very similar to the Cu-species T23-AlT1-Cu(I) and T23-AlT1HT4-Cu(I) (with and without adsorbed H_2). The binding energy and correspondingly the rotational hindrance at these sites are visibly reduced, Table 3, with tunnelling frequencies predicted in the range between 1.7 and 3.4 cm^{-1}, depending on the Al-Al distance.

Chabazite periodic models

The effect of neighbouring second framework Al atoms, at a different distances from the coordinated Cu-centre, in the same and different zeolite rings scenario was additionally tested by periodic structure calculations based on the Chabazite (CHA) zeolite type framework, using projector augmented plane wave representation of the electronic density in DFT. This structure was chosen due to its similarities with the MFI structure of ZSM-5 and the smaller unit cell, making the calculations feasible for the available computational power.
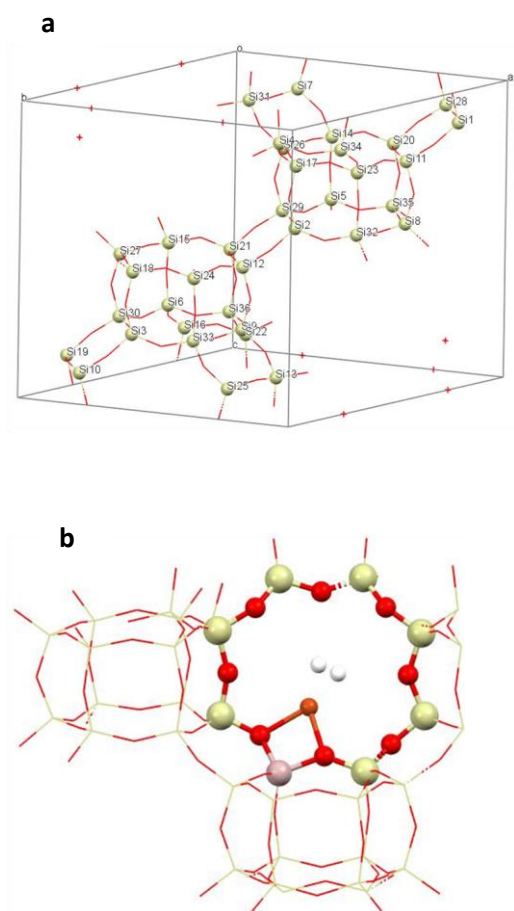
a

b

Figure 9. The Bravais unit cell of the CHA structure in P1 representation, with the total of 36 tetrahedral position, depicted in **a**). A monovalent Cu ion with H_2, is shown in **b**, with an Al-atom in the T12 position and the Cu-centre pointing inside the 8MR. Q_{ST} = 80 kJ/mol H_2, Ω_t **=0.85 cm^{-1}**

For all periodic calculations we used the conventional Bravais unit cell of the CHA structure, containing a total of 130 atoms. It must be pointed out that although the CHA structure contains only one crystallographically inequivalent site for Si (all SiO_4 equivalent), the local environment of the vicinal coordinated Cu-ions, compensating for Al-atoms replacing a Si atom is quite different. The diversity in environments becomes even larger if a second Al atom is introduced

in the place of a silicon. The original structure of the CHA framework (https://america.iza-structure.org/IZA-SC/framework.php?STC=CHA) was first fully optimized, i.e. all atomic coordinates and lattice parameters were allowed to vary. Then for the model with Al-substitutions and Cu centres we removed all symmetry restrictions, except the translational invariance of the unit cell, by reducing the original space group symmetry, R-3m, to group P1. The unit cell of the structure depicting the now inequivalent 36 tetrahedral sites occupied by Si, which could all individually or in different combination be replaced by Al atoms, is shown in Figure 9a. During the optimisation of the Al-substituted structures, with Cu-centres, with or without adsorbate guests, we allowed all atomic coordinates to be varied, along with isotropic lattice vectors change, i.e. the shape of the unit cell was kept constant to minimize effect of artificial Al(Cu-sites) long range ordering. When the Al-atom is in a T_{12} position, the extra framework Cu-ion may coordinate differently: i) near two oxygen atoms, in the 8MR as in (Fig. 9b, ii) above the 6MR as shown in Fig. 10, iii) above the nearby 4 MR – in Fig. 11.

a

b

Figure 10. Geometry optimized CHA structures with: **a** - Al-atom in the T12 tetrahedral site with the Cu(I) ion coordinated in the middle of the 6MR, to four oxygen atoms from the ring, and **b** – the interaction with dihydrogen has caused a substantial movement of the Cu(I) centre above the plain of the 6MR and the coordination bond to one of the oxygen atoms has been lost. Q_{ST} = 34kJ/mol H_2, Ω_t=3.6 cm^{-1}.

be quite exothermic and local framework overheating is very likely. Fast hydrogen loadings may cause isolated copper ions aggregation and reduction to metallic clusters. The sites at the 4 membered rings are specific for the CHA structure while the position in the 8 MR, being large enough is generally representative of isolated Cu-ions, coordinated to two framework oxygens and could be used as a model site describing the dynamics of dihydrogen complexes formed in the 12MR, at the intersection of the straight and the sinusoidal channels of the MFI(ZSM-5) structure. The site at the 6 membered ring is similar to the Z6 ring in the MFI structure of ZSM-5, for instance.
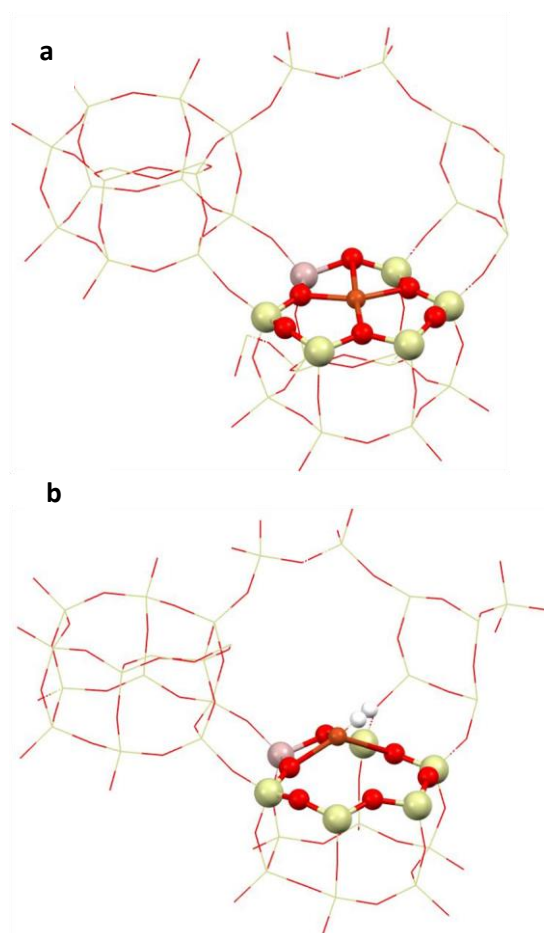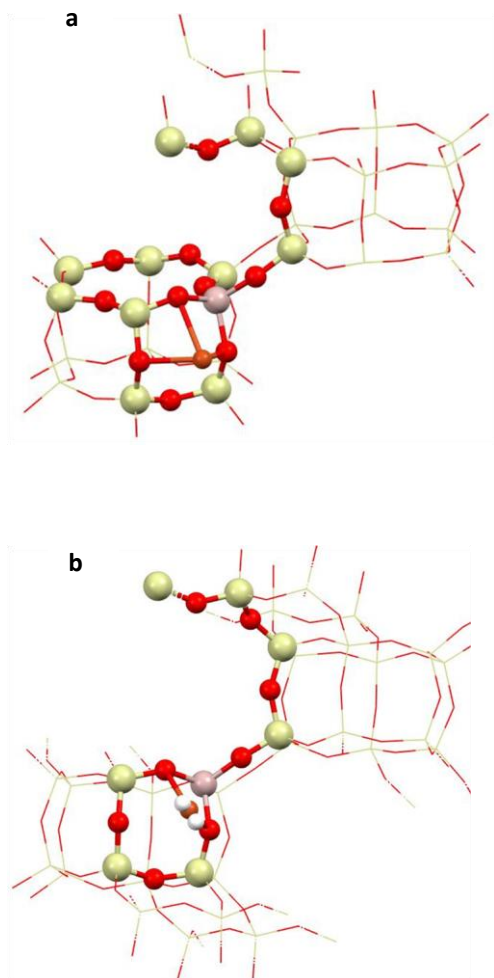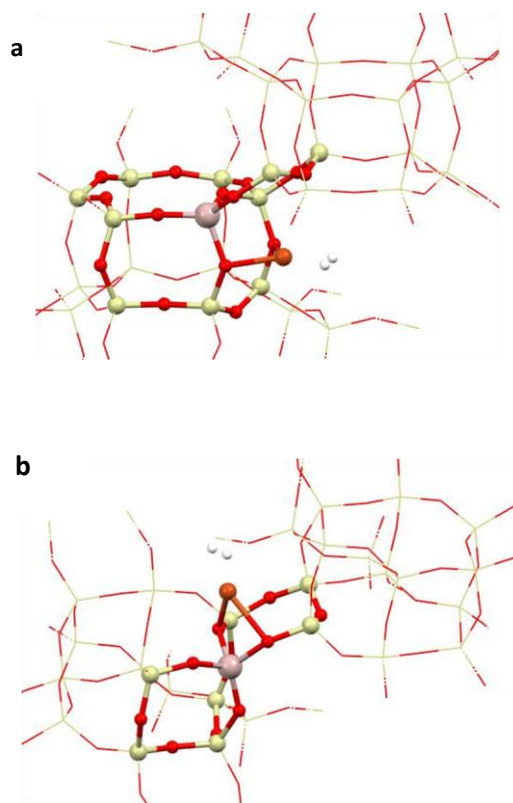

Figure 11. Geometry optimized CHA structures with: **a** - Al-atom in the T12 tetrahedral site with the Cu(I) ion coordinated above the 4MR at the wall created by the two 6MR. **b)** – when H_2 is bound by the Cu(I) center, again one coordinating bond to a nearby oxygen from the ring is lost and the H_2 ligand is positioned parallel to the other two coordinating oxygens. Q_{ST} = 69 kJ/mol H_2, Ω_t =3 cm^{-1}

Figure 12. Cu(I)-dihydrogen complexes on 4MR.

There is another, slightly higher energy site formed on the 4 MR, at the other side of the Cu-centre, where the nearest oxygen atom is below the plane defined by the four tetrahedrals. Consequently, the Cu-ion is coordinated to two oxygen atoms bridging the two 6MRs as shown in Fig. 12**a**. In the same figure, Fig.12**b**, is shown another site that is practically equivalent to the one in Fig. 11. For high Si/Al ratios, at low metal exchange levels, these sites represent the three possible types of sites for the extra framework Cu-ions and the corresponding dihydrogen complexes. It is worth noting that they reside very closely, a few Å away from each other, and especially when there is dihydrogen adsorbed, are quite similar in energy, Table S1, differing by just a few kJ/mol. This implies that the formed Cu(I) – dihydrogen complex may be rather mobile in the CHA structure, at moderate temperatures. Note that the adsorption of hydrogen is expected to

Next we turn to a structure with two Al -atoms: one again in the T_{12} position and second just opposite on the 8MR, which is actually a part of the lower 6MR if considering the same unit cell, in T_{30}, Fig. 13 and Fig. 9 **a** . The charge on the second Al-atom, in T_{30}, was compensated by a H-atom bound at the near O. In this coordination environment the Cu(I)-H_2 complex has the typical geometry features and stability, Tables S1 and S2. Notably, when the charge balancing proton, near the second Al in position T_{30}, is removed the Cu $-$ H distances in the complex are increased, the stability decreased by a few kJ/mol and the corresponding tunnelling frequency is substantially increased from 0.55 cm^{-1} in the Cu(I) complex up to 0.81 cm^{-1} for the formally designated as Cu(II) complex. It is worth noting that the corresponding dihydrogen complex is again diamagnetic, Table S1, specifying that in all two Al-atoms containing structures the two spin channels were treated separately.   Other examples from Table S1 are illustrated in Figure 14, with Al -atoms in T12 and T4, the latter again balanced by a proton, Fig. 14**a**, leading to a diamagnetic

Cu(I) species in either with or with no bound H_2, and a corresponding tunneling transition expected at 0.44 cm^{-1}. Fig. 14 **b** shows a structure with Al-atoms even further apart – in T_{12} and T_{34} and no charge balancing proton, i.e. expectedly a Cu(II) species. However, in this case too, the binding energy is significant, 69 kJ/mol, similar to that for the AlT$_4$HT$_{12}$Cu+H$_2$ structure – 82 kJ/mol H$_2$. The frequency of the tunnelling transition in AlT$_{12}$T$_{34}$ – coordination is shifted upwards at 1.38 cm^{-1}.

The weakest Cu-dihydrogen interactions occur at the 6MR where two Al-atoms reside in the ring as shown in Fig. 15, and the Cu-centre manifests a typical Cu(II) chemistry, with the usual half-empty 3d$_9$ orbital, atomic magnetic moment of about 0.8 Bohr, in a nearly square planar coordination. Interaction with H$_2$ leads to a typical physisorption adduct with binding energy of just below 18 kJ/mol and Cu-H distances about 2.5 Å, Tables S1 and S2. The corresponding rotational tunnelling transition is expected near 46 cm^{-1}, similarly to the cases of dihydrogen in HKUST-1 [54] and CPO-27-Cu [55]
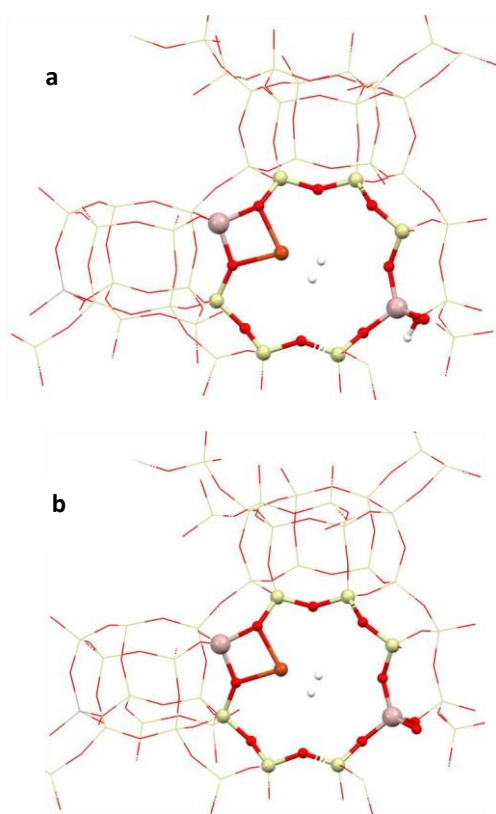

Figure 13. Cu-dihydrogen complex in the 8MR with Cu(I)-center near the T_{12} tetrahedral and a second Al-atom in T_{30}, charge balanced by a proton – **a,** the charge balancing proton removed in **b.**

Furthermore, we explored the binding of dihydrogen at dual Cu – species [21-24], of the types [Cu-O-Cu] and [Cu-OO-Cu] in the 8MR, as depicted in Fig. 16. Such structures could not be a priori ignored, particularly for the SA12 samples with relatively high Al-content and higher Cu-loadings, e.g. >1 %wt. The interactions between such structures, Fig. 16, and dihydrogen, however, turns out from our calculations, of purely dispersive origin, resulting in binding energies

of about 14 kJ/mol H$_2$, and Cu-H distances of 2.8 Å, like those in the CPO-27-Cu-dihydrogen system [55]. These appear equivalent to planar triangular and square Cu(II) species, as far the interactions with dihydrogen are concerned.
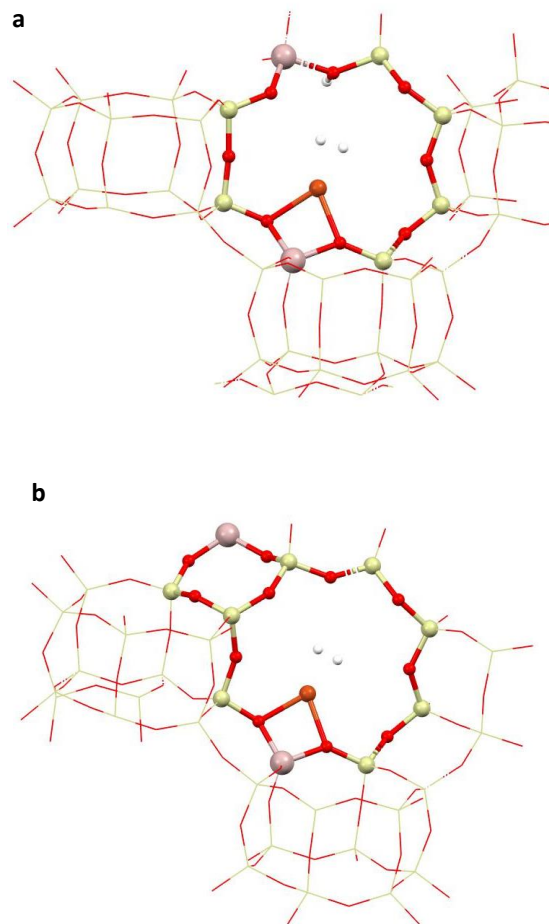
Figure 14. **a** - AlT$_4$HT$_{12}$Cu+H$_2$, Ω_t = 0.44 cm^{-1}, **b** - AlT$_{34}$T$_{12}$Cu+H$_2$, Ω_t = 0.98 cm^{-1}.

Various configurations of single and double aluminum atom substituted CHA structures, with one Cu-centre and where the second Al-atom is or not balanced by a proton, are detailed in Tables S1 and S2. These results show that the energetics and dynamics of the bound hydrogen is scattered over a broad range of energies, spanning typical physisorption values, c.a. 10 kJ/mol H$_2$, passing through an intermediate region of mixed contribution e.g. 30 kJ/mol, and reaching typical covalent interactions as strong as 80 kJ/mol H$_2$. In all cases, these binding energies are overestimated as compared to the experimental adsorption heats shown in Tables 1 and 2. The corresponding H$_2$ ligand rotational transitions are correspondingly covering the whole range of transition energies from just fractions of a cm^{-1}, for H$_2$ on Cu-species with low coordination number, e.g. 2, either near one Al atom or two, where the second is charge balance by a compensating proton.

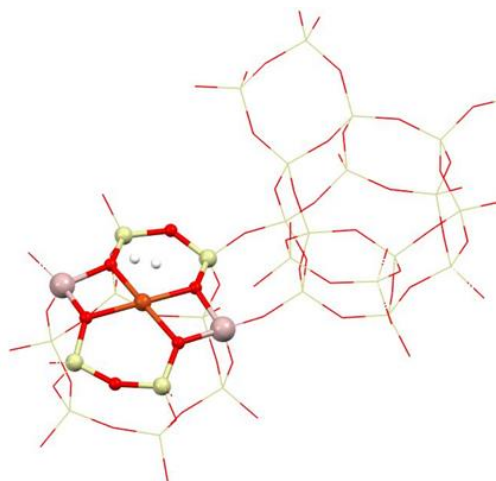**Figure 15.** Al in T_{12} and T_{27} in the 6MR of the CHA structure, with the Cu-center in a square planar coordination, in a weak physical adduct with H_2. E_b=17.6 kJ/mol H_2, Ω_t = 46 cm^{-1}.
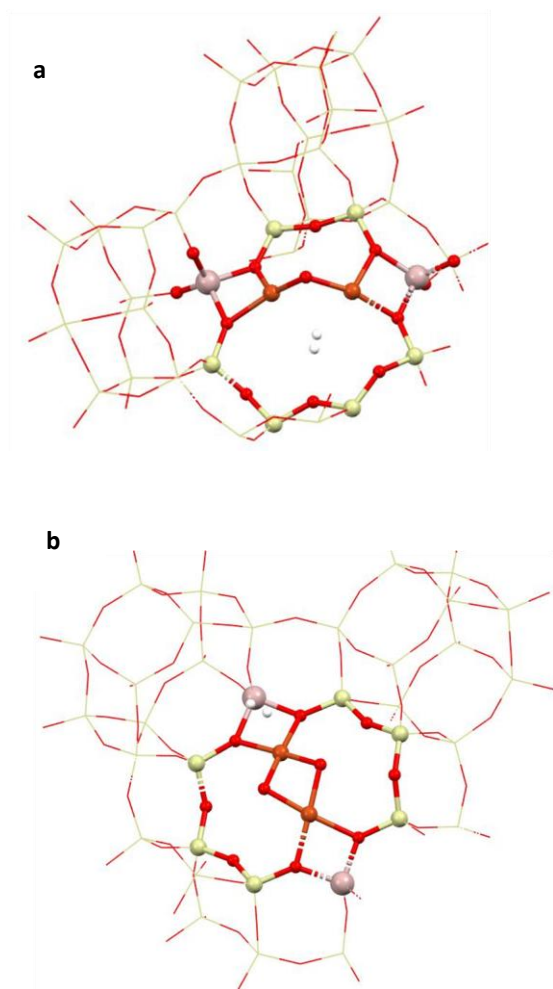
a

b

Figure 16. Dual Cu-species in the 8MR bridged by one oxygen atom in **a**, and two O-atoms in **b**.

It is quite remarkable that such species seem to manifest themselves by appearing all at very similar energies corresponding to the relatively sharp rotational feature in the INS spectra of high silica samples, at about 0.8 cm^{-1} [27], within both the cluster MFI-derived and the periodic Cha models, and in the present data, Fig. 6 a and b. Further up with the transition energy, 1 to a few cm^{-1}, come those sites where two framework Al-atoms are balanced by a single Cu-centre, lying in the larger zeolite rings e.g. the AlT$_{30}$T$_{12}$Cu^{2+}8MR, AlT$_4$T$_{12}$Cu^{2+}8MR, AlT$_{29}$T$_{12}$Cu^{2+}8MR, AlT$_{34}$T$_{12}$Cu^{2+}8MR, Table S1 and S. This sort of Cu-coordination must be responsible for the scattered intensity into the broad spectrum of rotational energies experimentally seen for the overexchanged ZSM-5[27] and here in Fig. 6. On the smaller rings e.g. the Z6 rings in ZSM-5, here the double 6MR and the 4MR, the Cu-center is in the vicinity of a larger number of atoms from the framework and the corresponding Cu-H$_2$ complexes are less stable, e.g. AlT$_{12}$Cu$^+$6MR and AlT$_{12}$Cu$^+$4MR, AlT$_{30}$HT$_{12}$Cu$^+$6MR, for which the rotational transitions fall above a few and below 10 cm^{-1}. No significant intensity in that range was observed neither in the present studies nor in our earlier experiments [27]. Fig. 7, however, displays, quite significant inelastic intensity in the range 40 ÷ 70 cm^{-1}. An inspection of Table S2 leads to the conclusion that these must originate from structures in which the Cu-dihydrogen complex is coordinated to a larger number of nearby oxygen atoms e.g. 4, with model representatives AlT$_{18}$T$_{12}$Cu^{2+}6MR, the AlT$_{27}$T$_{12}$Cu^{2+}6MR in Fig. 15, AlT$_{29}$T$_{12}$Cu^{2+}6MR, AlT$_{30}$T$_{12}$Cu^{2+}6MR, AlT$_{33}$T$_{12}$Cu^{2+}6MR.

A further important note to make, based on the total electronic energies data reported in Table S1, is that the stability of the Cu-sites, and the corresponding dihydrogen complexes are rather similar from site to site, differing by a few and up to a few tens of kJ/mol. Notably the monovalent Cu-species on the six membered ring with Al-atom in the T12 position is by about 60 kJ/mol more stable than above the 4MR and 38 kJ/mol more stable with respect to Cu(I) in the 8MR. Quite remarkably, when the corresponding dihydrogen complex is formed, the site above the 6MR becomes destabilized with respect to the neighbouring sites being higher in energy by 8kJ/mol with respect to the Cu(I)-H$_2$ complex in the 8MR. This latter site can be reached via the appearing as an intermediated state 4MR at just 26 kJ/mol higher than for the Cu-H$_2$ complex at the 6MR. Considering the relatively large isosteric heat released during the formation of the corresponding Cu-dihydrogen complexes, and the poor heat conductivity of the porous zeolite framework, one must expect large enough local adsorption related temperature jumps, leading to Cu-species and Cu-H$_2$ moieties migration withing the framework, possibly even Cu-ion reduction and clustering in extreme cases. Thus, even at low Cu exchange levels one may expect to find the Cu-centres in all possible coordination environments around the framework Al-atoms. This is particularly true when the Cu-exchanged material has been in contact with strong ligands as CO, NO$_x$, etc., which interact via significant covalent interactions with the Cu-centers and exert strong trans effects weakening the bonding between the centre and the framework, but may also happen during initial activation stages of water desorption, for instance. However, it is the Al-distribution in the parent zeolite framework that is the prerequisite of materials of different properties/activities. Indeed, the sitting and distribution of framework Al-atoms has already been established as a major factor in the catalytic activity of various zeolite structures and the reactivity

of the extra framework ions [60]. Recently two types of Cu-species have been anticipated in Cu-exchanged SSZ-13 [61] too, where only one crystallographic type of site has previously been detected by direct microscopic methods [62, 63]. Contrary to the earlier results a more recent synchrotron X-ray spectroscopy study showed [62] that only up to 20% of Cu(II) ions reside in the 6 membered rings of CHA zeolite with a Si-to Al ratio of 15.5 and Cu-to-Al loading of 0.45, while the rest 80% are located in 8-mebered rings. In this latter case, although crystallographically similar, the sites for the Cu-ion, and respectively the cation activity on these sites, would differ depending on the relative Al-Al distribution, as shown in our model calculations. Our simulations results support the idea that all of the above experimental results, at the macro-[60] and microscopic level [62, 63] are not contradictive, but simply observe different distribution of the Cu-species in the vicinity of the framework Al-atoms in various coordination environments – a distribution that could be influenced by different sample treatments and activation procedures. It is worth noting, that in practical applications, as in automotive catalytic converters for instance, these materials operate at elevated temperatures, e.g. $250 \div 350$ °C, where the zeolitic framework internal surface potential corrugation would be further reduced by the temperature and the heat effects of the interactions with the incoming gas constituents and products. Thus, it makes sense to anticipate that many of the above studied Cu-species contribute to the experimentally observed catalytic activities either as individual centres and/or in a cooperative manner. Furthermore, these findings point to the perspective of molecular dynamics studies on the mobilities of the above species, capable of elucidating the processes behing catalyst degradation and deactivation.

Conclusions

Adsorption isotherms of dihydrogen were measured at ambient temperatures, in two types of ZSM-5 zeolites with Si-to-Al ratios of 11.5 and 25. For both Si-to-Al ratios tested, the isosteric heats of adsorption increase 3 to 4 folds as compared to the bare H-ZSM-5, from about 8-9 kJ/mol H_2 to $24 - 37$ kJ/mol H_2 remaining still much lower than those previously found in the same zeolite type, but with a high copper exchange level [29]. From the room temperature measured dihydrogen sorption capacities becomes clear that higher fraction of strongly binding sites can be formed for higher Cu-exchange levels and higher Si-to-Al ratio.

The materials were also characterized by FTIR spectroscopy of in situ adsorbed CO (for characterization of Cu(I) sites) and NO (for characterization of Cu(II) sites). In all samples two types of Cu(I) species were found, able to coordinate up to two and up to three CO molecules, respectively. The relative concentrations of these sites depend on the parent zeolite local structure and copper loading. NO adsorption revealed the presence of isolated Cu(II) sites in all samples too, showing some degree of inhomogeneity.

Using DFT cluster and periodic model calculations, we have also shown that the observed INS bands may be explained in terms of two different types of Cu(I) species representing two relatively strong binding sites. The first group being the already known Cu(I) species coordinated to two oxygen atoms only. The broader INS feature is now suggested to originate from H_2 adsorbed on Cu-centres that compensate two framework Al-atoms, relatively far apart from each other so that after the activation process the compensating Cu-ions remain coordinated to only two O-atoms, near one of the Al-atoms. The activation of these sites must involve only thermal desorption of H_2O molecules, coordinated at Cu species during the exchange procedures, without the formation of bridging hydroxyls. Judging from the integral area of the INS peak at ~ 0.8 cm-1 and the broad band centred at ~ 1.4 cm-1, the amount of such Cu(I) centres, in place of the expected Cu(II) ones, must be quite significant and, possibly, even represent the majority of the strongly binding (reactive) Cu sites. Moreover, there must be a relatively broad spread of such Cu-species, replicating a variety of Al-Al distances in the MFI zeolite framework, offering even a larger possible spread than the studied here model CHA structure. The non-reduced Cu(II) species, most likely coordinated to 4 O-atoms, bind H_2 weakly, with adsorption energies in the range typical for physisorption as also previously observed for Cu-containing MOFs and zeolites.

Our study supports the view that depending on the Al content and relative disposition, a variety of both divalent and monovalent Cu-species may be present. Both species represent quite different activities towards guest molecules, ranging from typical physisorption to strong chemisorption, depending on the coordination mode. Hence, key feature, underlying the activity towards guest molecules of the various Cu-species in these zeolites, via their coordination environment and electronic states, possibly also readiness for switching between electronic states, is the Al content and relative geometric Al – Al configuration in the zeolite structure.

Conflicts of interest

There are no conflicts to declare.

Acknowledgements

References

[1] M. Iwamoto, H. Furukawa, Y. Mine, F. Uemura, S. Mikuriya, S. Kagawa, Copper(II) ion-exchanged ZSM-5 zeolites as highly active catalysts for direct and continuous decomposition of nitrogen monoxide. Chem Comm 1986; 1272-1273.

[2] M. Iwamoto, H. Yahiro, Novel catalytic decomposition and reduction of NO. Catal Today 1994;22:5-18.

[3] J. O. Petunchi, G. Sill, W. K. Hall," Studies of the selective reduction of nitric oxide by hydrocarbons. Appl Catal B 1993;2:303-321.

[4] M. Shelef, Selective Catalytic Reduction of NOx with N-Free Reductants. Chem Rev 1995;95:209-25.

[5] W. K. Hall, J. Valyon, Mechanism of NO decomposition over Cu-ZSM-5. Catal Lett 1992;15:311-315.

[6] J. Dědeček and B. Wichterlová, Siting and Redox Behavior of Cu Ions in CuH-ZSM-5 Zeolites. Cu^+ Photoluminescence Study. J Phys Chem 1994;98:5721-5727.

[7] J. Dědeček, Z. Sobalik, Z. Tvarůžková, D. Kaucký and B. Wichterlová, Coordination of Cu Ions in High-Silica Zeolite Matrixes. Cu^+ Photoluminescence, IR of NO Adsorbed on Cu^{2+}, and Cu^{2+} ESR Study. J Phys Chem 1995;99:16327-37.

[8] B. Wichterlová, J. Dědeček, Z. Sobalik, A. Vondrová, and K. Klier, On the Cu Site in ZSM-5 Active in Decomposition of NO: Luminescence, FTIR Study, and Redox Properties. J Catal 1997;169:194-202.

[9] C. Lamberti, S. Bordiga, M. Salvaggio, G. Spoto, A. Zecchina, F. Geobaldo, G. Vlaic, M. Bellatreccia, XAFS, IR, and UV–Vis Study of the Cu^I Environment in Cu^I-ZSM-5. J Phys Chem B 1997;101: 344-60.

[10] G.T. Palomino, P. Fisicaro, E. Giamello, S. Bordiga, C. Lamberti, A. Zecchina, Oxidation States of Copper Ions in ZSM-5 Zeolites. A Multitechnique Investigation. J Phys Chem B 2000;104:4064-73.

[11] F.X. Llabres I Ximena, P. Fisicaro, G. Berlier, A. Zecchina, G.T. Palomino, C. Prestipino, S. Bordiga, E. Giamello, C. Lamberti, Thermal Reduction of Cu^{2+}–Mordenite and Re-oxidation upon Interaction with H_2O, O_2, and NO. J Phys Chem B 2003;107:7036-44.

[12] Y. Kuroda, K. Yoshikawa, R. Kumashiro, M. Nagao, Analysis of Active Sites on Copper Ion-Exchanged ZSM-5 for CO Adsorption through IR and Adsorption-Heat Measurements. J Phys Chem B 1997;101:6497-503.

[13] R. Kumashiro, Y. Kuroda, M. Nagao, New Analysis of Oxidation State and Coordination Environment of Copper Ion-Exchanged in ZSM-5 Zeolite. J Phys Chem. B 1999;103:89-96.

[14] Y. Kuroda, R. Kumashiro, A. Itadani, M. Nagao, H. Kobayashi, A more efficient copper-ion-exchanged ZSM-5 zeolite for N_2 adsorption at room temperature: Ion-exchange in an aqueous solution of $Cu(CH_3COO)_2$. Phys. Chem. Chem. Phys. 3 (2001) 1383-1390.

[15] H. van Koningsveld, H. van Bekkum, J.C. Jansen, On the location and disorder of the tetrapropylammonium (TPA) ion in zeolite ZSM-5 with improved framework accuracy. Acta Cryst B 1987;43:127-132.

[16] D. Nachtigalová, P. Nachtigal, M. Sierka and J. Sauer, „Coordination and siting of Cu^+ ions in ZSM-5: A combined quantum mechanics/interatomic potential function study. Phys Chem Chem Phys 1999;1:2019-26.

[17] P. Nachtigal, D. Nachtgalová and J. Sauer, Coordination Change of Cu^+ Sites in ZSM-5 on Excitation in the Triplet State: Understanding of the Photoluminescence Spectra. J Phys Chem B 2000;104:1738-45.

[18] P. Nachtigal, D. Nachtgalová and J. Sauer, Coordination of Cu^+ and Cu^{2+} ions in ZSM-5 in the vicinity of two framework Al atoms. Phys Chem Chem Phys 2001;3: 1552-9.

[19] M. Davidova, D. Nachtgalova, R. Bulanek and P. Nachtigal, Characterization of the Cu^+ Sites in High-Silica Zeolites Interacting with the CO Molecule: Combined Computational and Experimental Study, J Phys Chem B 2003;107:2327-32.

[20] B. Xing, J. Ma, R. Li, H. Jiao, Location, distribution and acidity of Al substitution in ZSM-5 with different Si/Al ratios – a periodic DFT computation. Catal Sci Technol 2017;7: 5694-708.

[21] M. A. C. Markovits, A. Jentys, M. Tromp M. Sanchez-Sanchez, J. A. Lercher, Effect of Location and Distribution of Al Sites in ZSM-5 on the Formation of Cu-Oxo Clusters Active for Direct Conversion of Methane to Methanol. Top Catal 2016;59: 1554–63.

[22] G. Li, P. Vassilev, M. Sanchez-Sanchez, J. A. Lercher, E. J. M. Hensen, E. A. Pidko, Stability and reactivity of copper oxo-clusters in ZSM-5 zeolite for selective methane oxidation to methanol. J Catal 2016;338:305-12.

[23] Isolation of the Copper Redox Steps in the Standard Selective Catalytic Reduction on Cu-SSZ-13. Angew Chem Int Ed 2014;53:11828–33.

[24] A. R. Fahami, T. Günter, D. E. Doronkin, M. Casapu, D. Zengel, T. H. Vuong, M. Simon, F. Breher, A. V. Kucherov, A. Brückner. J.-D. Grunwaldt The dynamic nature of Cu sites in Cu-SSZ-13 and the origin of the seagull NO_x conversion profile during NH3-SCR. React Chem Eng 2019;4:1000-18.

[25] X. Solans-Monfort, V. Branchadell, M. Sodupe, C. M. Zicovich-Wilson, E. Gribov, G. Spoto, C. Busco, P. Ugliengo, Can Cu^+-Exchanged Zeolites Store Molecular Hydrogen? An Ab-Initio Periodic Study Compared with Low-Temperature FTIR. J Phys Chem B 2004;108:8278-86.

[26] A. Serykh, V.B. Kazansky, Unusually strong adsorption of molecular hydrogen on Cu^+ sites in copper-modified ZSM-5. Phys Chem Chem Phys 2006;6:5250-5.

[27] P. A. Georgiev, A. Albinati, B. Mojet, J. Ollivier, J. Eckert, „Observation of Exceptionally Strong Binding of Molecular Hydrogen in a Porous Material: Formation of an η^2-H_2 Complex in a Cu-Exchanged ZSM-5 Zeolite. J Am Chem Soc 2007;129:8086-7.

[28] G. J. Kubas, Fundamentals of H_2 Binding and Reactivity on Transition Metals Underlying Hydrogenase Function and H_2 Production and Storage. Chem Rev 2007;107:4152-205, Activation of dihydrogen and coordination of molecular H_2 on transition metals. J Organomet Chem 2014;751:33-49.

[29] P. A. Georgiev, A. Albinati, J. Eckert, Room temperature isosteric heat of dihydrogen adsorption on Cu(I) cations in zeolite ZSM-5. Chem Phys Lett 2007;449:182-5.

[30] I. Altiparmak, B. Karakaya, D. Uner, B. Ipek, H_2 adsorption on Cu(I)-ZSM-5: exploration of Cu(I)-exchange in solution. Int J Hydrogen Energy 2019;44:18866e74.

[31] B. Ipek, I. Altiparmak, Remarkable isosteric heat of hydrogen adsorption on Cu(I)-exchanged SSZ-39. Int J Hydrogen Energy 2020; In press, DOI: 10.1016/j.ijhydene.2020.03.083

[32] R. Xionga, L. Zhangb, P. Lia, W. Luoa, T. Tanga, B. Aoc, G. Sanga, C. Chena, X. Yana, J. Chenc, M. Hirscher, Highly effective hydrogen isotope separation through dihydrogen bond on Cu(I)-exchanged zeolites well above liquid nitrogen temperature. Chem Eng J 2020;391:123485, 10pp.

[33] J. Olivier, M. Plazanet, H. Schober, J.C. Cook, First results with the upgraded IN5 disk chopper cold time-of-flight spectrometer. Physica B 2004;350:173-7; J. Ollivier, H. Mutka, L. Didier, The New Cold Neutron Time-of-Flight Spectrometer IN5. Neutron News 2010;21:22-5.

[34] T. Unruh, J. Neuhaus, W. Petry, The high-resolution time-of-flight spectrometer TOFTOF. Nuclear Instruments and Methods in Physics Research Section A: Accelerators, Spectrometers, Detectors and Associated Equipment 2007;580:1414-22.

[35] M. J. Frisch, G. W. Trucks, H. B. Schlegel, G. E. Scuseria, M. A. Robb, J. R. Cheeseman, G. Scalmani et al. Gaussian 09

[36] T.G. Golden, S. Sircar, „Gas Adsorption on Silicalite. J Colloid Int Sci 1994;162: 182-8.

[37] C. Otero-Areán, M. Rodriguez Delgado, G. Turnes Palomino, M. Tomás Rubio, N. M. Tsyganenko, A. A. Tsyganenko, E. Garrone, Thermodynamic studies on hydrogen adsorption on the zeolites Na-ZSM-5 and K-ZSM-5. Microporous Mesoporous Mater. 2005;80:247-52.

[38] T. Pieplu, F. Poignant, A. Vallet, J. Saussey, J. C. Lavalley, J. Mabilon, Oxidation state of copper during the reduction of NOx with propane on H-Cu-ZSM-5 in excess oxygen. Stud Surf Sci Catal 1995;96:619-29.

[39] G. Spoto, A. Zecchina, S. Bordiga, S. Ricchiardi, G. Martra, G. Leofanti, G. Petrini, Cu(I)-ZSM-5 zeolites prepared by reaction of H-ZSM-5 with gaseous CuCl: Spectroscopic characterization and reactivity towards carbon monoxide and nitric oxide. Appl. Catal. B 1994;3:151-72.

[40] K. Hadjiivanov, H. Knözinger, FTIR Study of Low-Temperature CO Adsorption on Cu-ZSM-5: Evidence of the Formation of $Cu^{2+}(CO)_2$ Species. J Catal 2000;191: 480–5.

[41] K. Hadjiivanov, M. Kantcheva, D. Klissurski, IR study of CO adsorption on Cu-ZSM-5 and CuO/SiO_2 catalysts: σ and π components of the Cu^+-CO bond. J Chem Soc Faraday Trans 1996;92:4595–600.

[42] K. Hadjiivanov, H. Knözinger, FTIR study of CO and NO adsorption and coadsorption on a Cu/SiO_2 catalyst: Probing the oxidation state of copper. Phys Chem Chem Phys 2001;3:1132-7.

[43] M. Kantcheva, K. Hadjiivanov, A. Davydov and A. Budneva, Low-temperature CO adsorption on Cu^{2+}/TiO_2 catalysts. Appl Surf Sci 1992;55:49-55.

[44] K. Hadjiivanov, G. Vayssilov, Characterization of oxide surfaces and zeolites by carbon monoxide as an IR probe molecule. Adv Catal 2002;47:307-511.

[45] N. Drenchev, M. H. Rosnes, P.D.C. Dietzel, A. Albinati, K. I. Hadjiivanov, and P. A. Georgiev, Open Metal Sites in the Metal–Organic Framework CPO-27-Cu: Detection of Regular and Defect Copper Species by CO and NO Probe Molecules. J Phys Chem C 2018;122:17238–17249.

[46] K. Hadjiivanov, Identification of Neutral and Charged NxOy Surface Species by IR Spectroscopy. Catal Rev Sci Eng 2000;42:71-144.

[47] Y. Fu, Y. Tian, P. Lin, A low-temperature IR spectroscopic study of selective adsorption of NO and CO on $CuO/γ-Al_2O_3$. J Catal 1991;132:85-91.

[48] G. Spoto, S. Bordiga, D. Scarano, and A. Zecchina, Well defined $Cu^I(NO)$, $Cu^I(NO)_2$ and $Cu^{II}(NO)X$ (X = O^- and/or NO^{2-}) complexes in Cu^I-ZSMS prepared by interaction of H-ZSM5 with gaseous CuCl. Catal Lett 1992;13:39-44.

[49] A. Zecchina, C. Otero-Arean, Diatomic molecular probes for mid-IR studies of zeolites. Chem Soc Rev 1996;25:187-97.

[50] N. Drenchev, P. A. Georgiev, K.I. Hadjiivanov, J. Mol. Catal. A: Chemical 2011;341:7-13.

[51] P.A. Georgiev, D.K. Ross, P. Albers, A.J. Ramirez-Cuesta, The rotational and translational dynamics of molecular hydrogen physisorbed in activated carbon: A direct probe of microporosity and hydrogen storage performance. Carbon 2006;44:2724-38.

[52] P. A. Georgiev, A. Giannasi, D.K. Ross, M. Zoppi, L.J. Sauvajol and J. Stride, Experimental Q-dependence of the rotational J = 0-to-1 transition of molecular hydrogen adsorbed in single-wall carbon nanotube bundles. Chem Phys 2006;328:318-23.

[53] S.S-Y. Chui, S.M-F. Lo, J.P.H. Charmant, A.G. Orpen, I.D. Williams, A Chemically Functionalizable Nanoporous Material $[Cu_3(TMA)_2(H_2O)_3]_n$. Science 1999;283:1148-50.

[54] C. M. Brown, Y. Liu, T. Yildirim, V. K. Peterson, C. J. Kepert, Hydrogen adsorption in HKUST-1: a combined inelastic neutron scattering and first-principles study. Nanotechnology 2009;20:204025, 11pp.

[55] M. H. Rosnes, M. Opitz, M. Frontzek, W. Lohstroh, J. P. Embs, P. A. Georgiev, P. D. C. Dietzel, Intriguing differences in hydrogen adsorption in CPO-27 materials induced by metal substitution. J Mater Chem A 2015;3:4827–39.

[56] P.D.C. Dietzel, P.A. Georgiev, J. Eckert, R. Blom, T. Strässle, T. Unruh, Interaction of hydrogen with accessible metal sites in the metal–organic frameworks $M_2(dhtp)$ (CPO-27-M; M = Ni, Co, Mg). Chem Commun 2010;46:4962-4.

[57] K. A. Forrest, T. Pham, P. A. Georgiev, F. Pinzan, C. R. Cioce, T. Unruh, J. Eckert, B. Space, Investigating H_2 Sorption in a Fluorinated Metal–Organic Framework with Small Pores Through Molecular Simulation and Inelastic Neutron Scattering. Langmuir 2015;31:7328-36.

[58] T. Pham, K. A. Forrest, P. A. Georgiev, W. Lohstroh, A. Hogan, B. Space, J. Eckert, A high rotational barrier for physisorbed hydrogen in an fcu-metal–organic framework. Chem Commun 2014;50:14109-14112.

[59] A.J. Ramirez-Cuesta, P.C.H. Mitchell, Hydrogen adsorption in a copper ZSM5 zeolite: An inelastic neutron scattering study. Catal Today 2006;120:368-73.

[60] J. Dědeček, Z. Sobalík, B. Wichterlová, Siting and Distribution of Framework Aluminium Atoms in Silicon-Rich Zeolites and Impact on Catalysis. Catal Rev Sci Eng 2012;54:135–223.

[61] J. H. Kwak, H. Zhu J. H. Lee, C. H. F. Peden, J. Szanyi, Two different cationic positions in Cu-SSZ-13?. Chem Commun 2012;48:4758–4760.

[62] D.W. Fickel, E. D'Addio, J. A. Lauterbach and R. F. Lobo, The ammonia selective catalytic reduction activity of copper-exchanged small-pore zeolites. Appl Catal B 2011;102:441- 448.

[63] C. W. Andersen, M. Bremholm, P. N. R. Vennestrøm, A. B. Blichfeld, L. F. Lundegaard, B. B, Iversen, Location of Cu^{2+} in CHA zeolite investigated by X-ray diffraction using the Rietveld/maximum entropy method. Int Un Cryst J 2014;1:382-6.

Supporting information for:

Dynamics of bound states of dihydrogen at Cu(I) and Cu(II) species coordinated near one and two zeolite framework aluminium atoms: A Combined Sorption, INS, IR and DFT study

P.A. Georgiev[a,e*], N. Drenchev[b], K. I. Hadjiivanov[b], J. Ollivier[c], T. Unruh[d]

and A. Albinati[e]

[a]*Condensed Matter Physics and Microelectronics Department, The University of Sofia, J. Bourchier 5, Sofia 1164, Bulgaria*
[b]*Instute of General and Inorganic Chemistry, Bulgarian Accademy of Sciences, G.Bonchev str, Sofia, Bulgaria*

[c]*Institute Laue-Langevin, 6 rue Jules Horovitz, BP156, F-38042 Grenoble Cedex 9,Grenoble, France.*
[d]*Institute of Condensed Matter Physics, Friedrich-Alexander-Universität Erlangen, Nürnberg, Germany.*
[e]*Istituto di Chimica dei Composti Organometallici (ICCOM) Sesto Fiorentino, Florence Italy and University of Milan, Milan, 19 Via C. Golgi, 20133 Milan, Italy.*

1. Full reference [27]

27. M.J. Frisch, G.W. Trucks, H.B. Schlegel, G.E. Scuseria,
 M.A. Robb, J.R. Cheeseman, G. Scalmani, V. Barone, B. Mennucci,G.A. Petersson, H.Nakatsuji, M. Caricato, X.Li, H.P. Hratchian, A.F. Izmaylov, J. Bloino, G. Zheng, J.L. Sonnenberg, M. Hada, M. Ehara, K. Toyota, R. Fukuda, J. Hasegawa, M. Ishida, T. Nakajima, Y. Honda, O. Kitao, H. Nakai, T. Vreven, J.A. Montgomery, Jr., J.E. Peralta, F. Ogliaro, M. Bearpark, J.J. Heyd, E. Brothers, K.N. Kudin, V. N. Staroverov, R. Kobayashi, J. Normand, K. Raghavachari, A. Rendell, J.C. Burant, S.S. Iyengar, J. Tomasi, M. Cossi, N. Rega, J.M. Millam, M. Klene, J.E. Knox, J.B. Cross, V. Bakken, C. Adamo, J. Jaramillo, R. Gomperts, R.E. Stratmann, O.Yazyev, A.J. Austin, R. Cammi, C. Pomelli, J.W. Ochterski,R.L. Martin, K. Morokuma, V.G. Zakrzewski, G.A. Voth,P. Salvador, J.J. Dannenberg, S. Dapprich, A.D. Daniels,O. Farkas, J.B. Foresman, J.V. Ortiz, J. Cioslowski, and D.J. Fox, Gaussian, Inc., Wallingford CT, 2009.

2. Dihydrogen adsorption isotherms in the H and Cu-exchanged forms of ZSM-5 zeolites CBV2314G with Si/Al=11.5 and CBV5524G with Si/Al=25
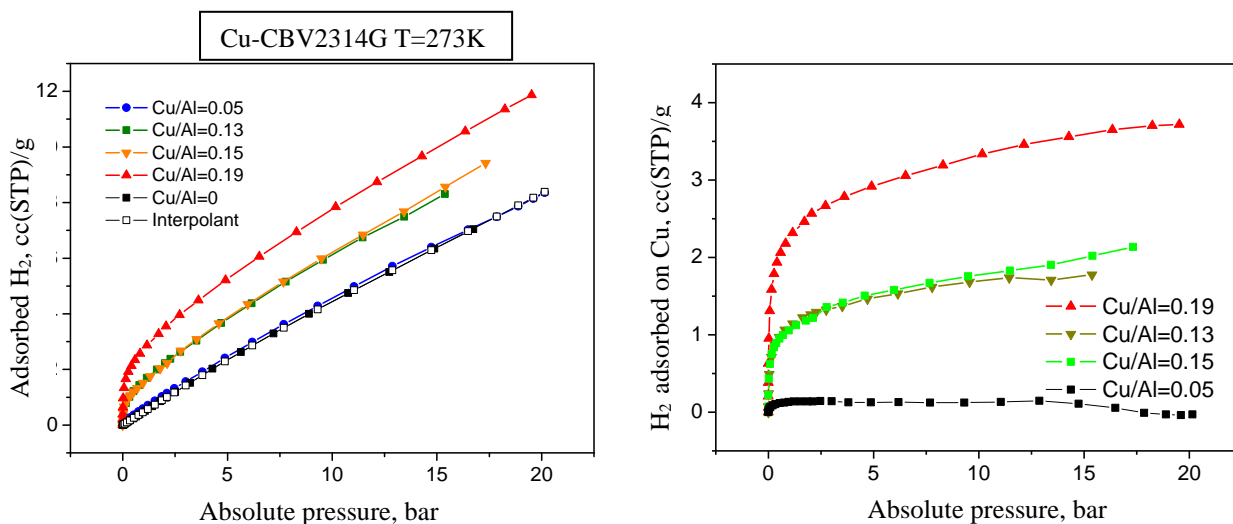
Figure S1. H$_2$ adsorption isotherms, measured at 273K, in the H-form, Cu/Al=0, and Cu-exchanged SA12 (CBV2314G) samples. The total amount of adsorbed dihydrogen at STP per gram material is shown in the left block while on the right side block is shown the subtracted adsorption isotherms, corresponding to the extra adsorption due to the presence of Cu-ions.
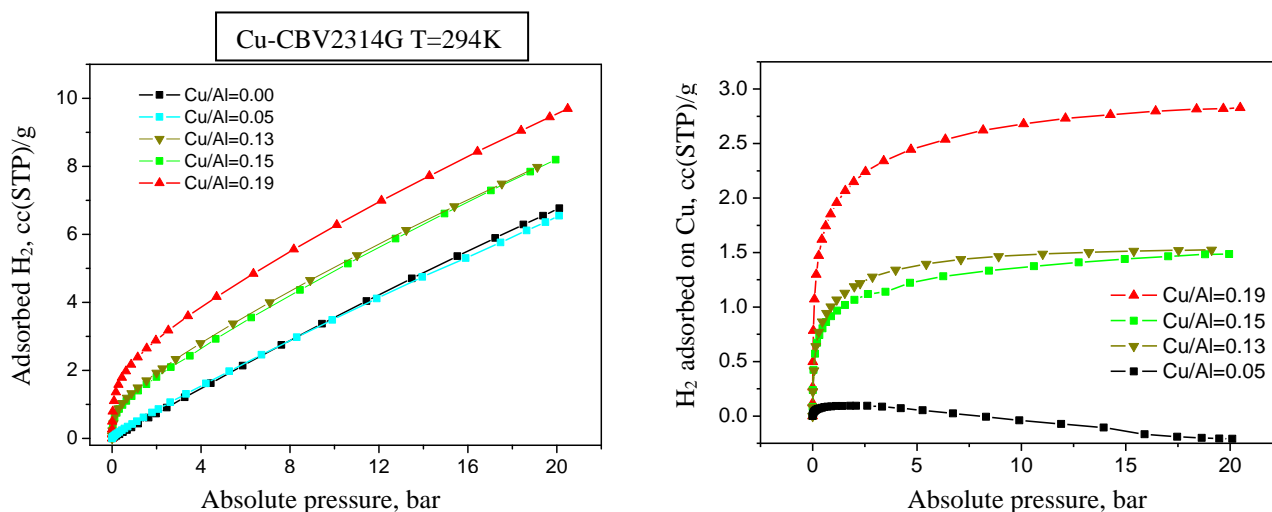
Figure S2. The same as in the previous figure for 294 K.
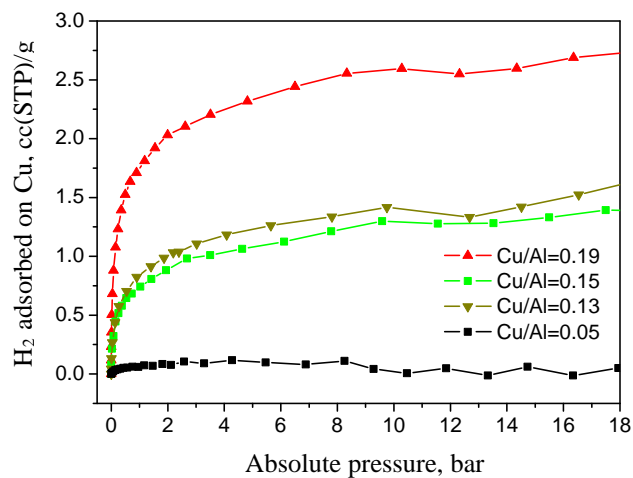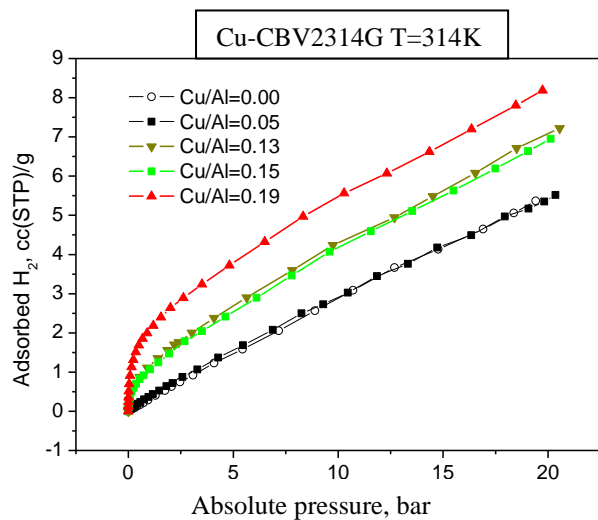
Figure S3. The same as in Figs 1 and 2, but for 314K.
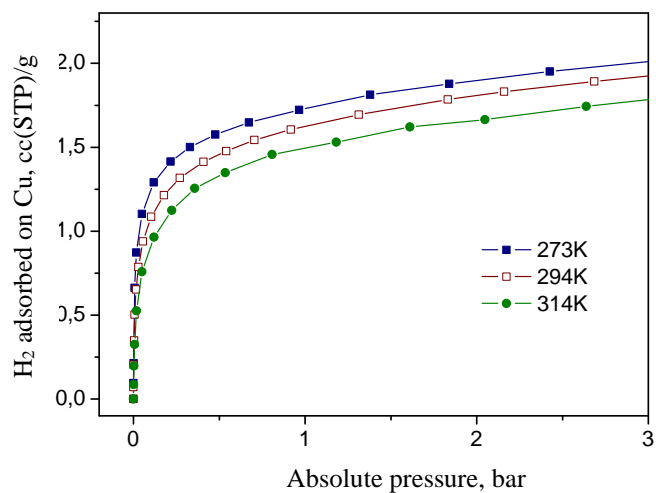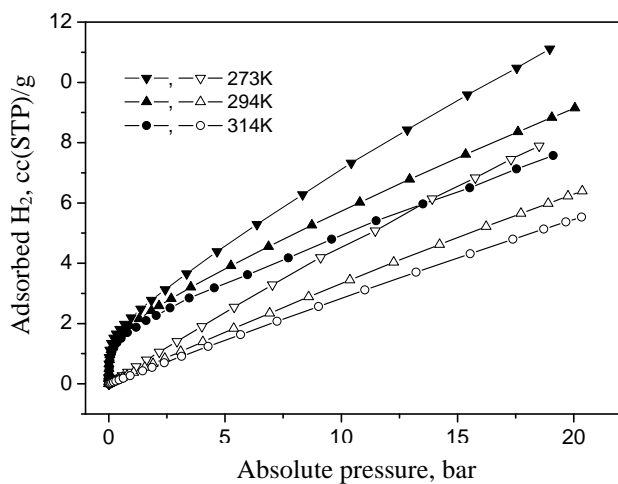
Figure S4. Dihydrogen adsorption isotherms in the H-form (left block, empty marks) and the Cu-exchanged (Cu/Al=25, SA25Cu0.25) forms of CBV5524G ZSM-5 zeolite at 273, 294, and 314 K as indicated in the figure's legends. The pure H-ZSM-5 subtracted isotherms are shown in the right-hand side block.
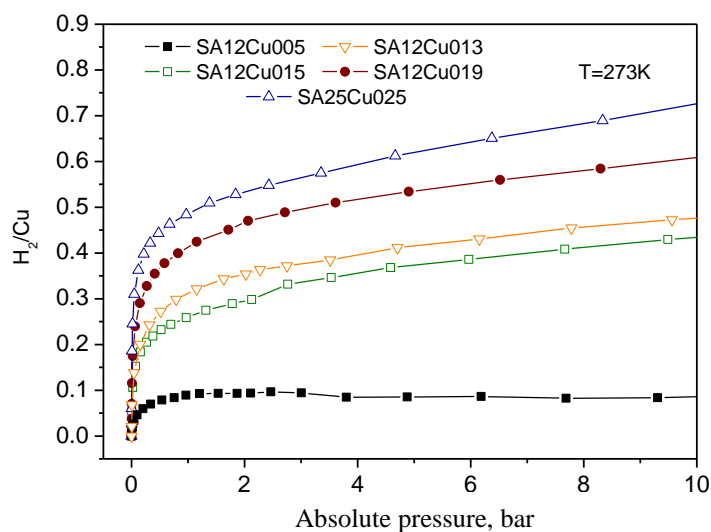
Figure S5. Dihydrogen adsorption isotherms, measured at 273K, in both Cu-exchnaged ZSM-5 materials for different Cu-exchange levels as indicated in the figure legend. The adsorption in the corresponding pure H-zeolite forms have been subtracted.

2. INS of H_2 adsorbed in pure H-ZSM-5, Si/Al=25(H-CBV5524)
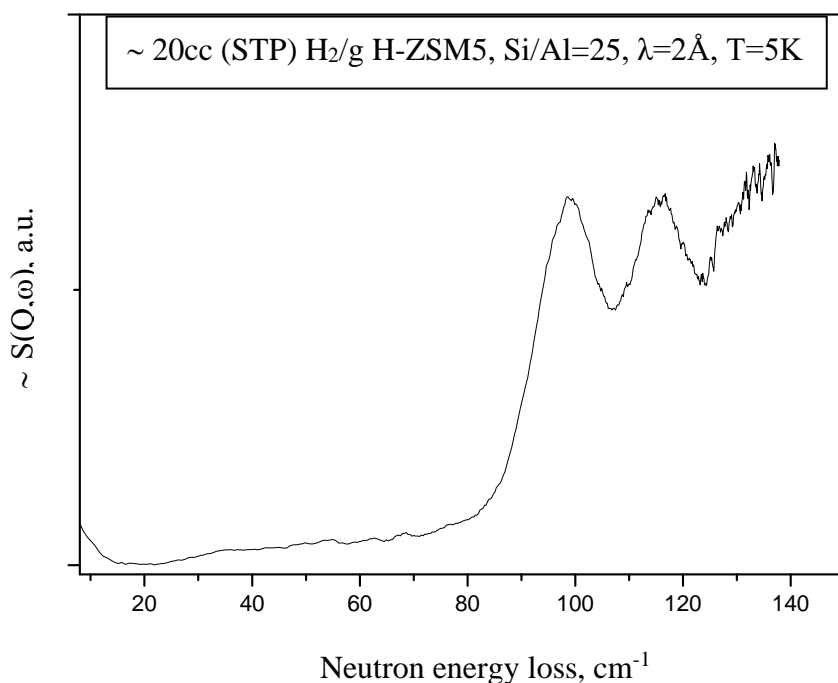
Figure S6. INS spectrum of about 1 mmol dihydrogen adsorbed in H-ZSM-5, CBV5524. Note the absence of the peaks in the range 40-70 cm^{-1} observed in the Cu-exchanged samples spectra.

3. DFT calculations

The multiprocessor version of Gaussian 09 computational package[S1] (revision A.02) has been used throughout the cluster model calculation in these studies. The total energy of each structural fragment has been calculated using the B3LYP[S2] hybrid functional. The electronic wave-function has been modelled using the following Gaussian basis sets: STO-3G minimal basis on terminal hydrogens, 6-31G(d,p) on O, Si, Al and charge compensating H atoms, 6-311+(d) on Cu, and the same supplied with diffuse and polarisation (2pd) functions on the hydrogen atoms in dihydrogen molecules. For each of the examined ZSM-5 clusters the terminal hydrogen atoms replaced corresponding Si atoms, and then only the terminal hydrogen positions were optimised by relaxing the O-H bond lengths. The positions of all other atoms except terminal H were kept fixed at their relative initial lattice positions[S3]. For the initial zeolite crystal structure parameters we used the atom positions by Koningsveld et al.[S3] and the lattice parameters from a recent neutron study[S4]. Aluminium atoms have then been added in the selected tetrahedral positions along with Cu and H-atoms were necessary. The charge compensating protons (H), Cu ion and the H_2 molecule coordinates have been optimised together with the coordinates of the other atoms except terminal OH groups. This partial optimisation technique had to be adopted in order to prevent deformation of the clusters causing too strong deviation from their shape in the original ZSM-5 structure. The disadvantage is that a number of negative frequencies are obtained along non-optimized variables which are excluded from the consequent vibrational energy corrections for all structures. Default integration grid size, energy and geometry convergence criteria have been used throughout these studies. Basis Set Superposition Errors (BSSE) have been estimated only at the equilibrium geometries of the optimised structures via the standard counterpoise method[S5] as implemented in Gaussian09.

Calculations involving periodic zeolite clusters were performed using the Abinit software package[S6,S7] version 8. The PBE parametrization of GGA was used for the total energy calcualtion. Spatially isotropic, i.e. angles between the lattice vectors were kept fixed, geometry optimizations for all investigated structures, with the Bravai unit cell of the Chabazite structure, with the space group reduced to P1, were done until the forces on all atoms were reduced to below 1 meV/Å. The projector augmented pseudopotential method[S8] was used to model the electronic wave function and electron-ion interactions, with an energy cut off on the plane wave part of 820 eV. Additionally, a Hubbard U correction on the energy of Cu 3d electrons was applied with a magnitude of 9 eV and a correlation part J of 1 eV,

computed for a free Cu^+-ion, using the standard Abinit procedure (**macro_uj=1**), treating the two spin channels separately as in all other calculations. The double counting term, calculated using the atomic limit method[S9] was used in all periodic calculations. This set up was used for both types of Cu-species in the model periodic structures. It is worth noting that the binding energy of H_2 and corresponding dynamics depends on the choice of U. Thus, with U=0, the binding energy of H_2 on Cu(I) in the CHA model CHA-Cu(I)Al1 rises up to 143 kJ/mol H_2 from 80.8 kJ/mol H_2 with U=9 eV. The method is however well suited for large scale calculations, especially on larger systems and behaves suitably for the calculation of the binding in porous Metal-Organic frameworks(MOFs), for instance, of zero spin molecules. [S10] Our fixed U -value is relatively high, but falls very close to previously calculated and tested values for the Cu_2O, Cu_4O_3, and CuO materials.[S11] Dispersive interactions between the Cu-centers and the H_2 molecules were taken into account with use of the Grimme's D3 correction[S12].

Dihydrogen rotational tunneling frequencies

The barrier to rotation, V_2, for H_2 molecules adsorbed at each type of Cu-species was calculated as the difference between the equilibrium state and the one in which the corresponding H_2 molecule is rotated by 90°. The corresponding Schrödinger equation in one dimension, the rotational angle φ, with a perturbation potential V of the form:

$$V = 1/2 V_2 \cos 2\varphi$$

is reduced to the well-known Mathieu equation which was solved numerically to obtain the rotational tunnelling frequencies, Ω_t, given in Table S2.

Table S1. Total energies of the calculated Cu-exchanged CHA-structures without and with H_2, Cu-coordination with distances to the nearest oxygens up to about 2.5 Å, before and after H2 adsorption, Cu-H and H-H distances in the dihydrogen complex.

Structure	Total Energy, Ha	Cu-O dist., [Å]	Cu-H dist., [Å] H-H dist., [Å]
$AlT_{12}Cu^+4MR$ +H_2	-1361.1826118227 -1362.3753050965	2.062, 2.234, 2.446 2.051, 2.248	1.671, 1.672 0.808
$AlT_{12}Cu^+6MR$ +H_2	-1361.2061062377 -1362.3855373378	1.999, 2.093, 2.241 2.044, 2.146	1.666, 1.669 0.809
$AlT_{12}Cu^+8MR$ +H_2	-1361.1917213372 -1362.3886351401	2.068, 2.103 2.061, 2.076	1.646, 1.654 0.815
$AlT_{29}Cu^+4MR$ +H_2	-1361.1924691526 -1362.3880968249	2.071, 2.218, 2.413 2.048, 2.113	1.655, 1.658 0.814
$AlT_{30}HT_{12}Cu^+6MR$ +H_2	-1359.9104751672 -1361.0887052934	2.010, 2.096, 2.238 2.053, 2.165	1.675, 1.677 0.806
$AlT_{30}HT_{12}Cu^+8MR$ +H_2	-1359.8945740618 -1361.0906550770	2.083, 2.156, 2.540 2.059, 2.121	1.659,1.667 0.813
$AlT_{30}T_{12}Cu^{2+}8MR$ +H_2	-1359.2490672993 -1360.4442433760	2.470, 2.085, 2.045 2.060, 2104	1.682, 1.695 0.808
$AlT_4T_{12}Cu^{2+}8MR$ +H_2	-1359.2473824473 -1360.4433784381	2.048, 2.066 2.036, 2.118	1.668, 1.712 0.808
$AlT_4HT_{12}Cu^{2+}8MR$ +H_2	-1359.8833482755 -1361.0788113787	2.104, 2.233, 2.246 2.060, 2.083	1.646, 1.648 0.819
$AlT_{17}T_{12}Cu^{2+}8MR$ +H_2	-1359.2724355412 -1360.4606763460	1.959, 1.996, 2.050 1.990, 2.002, 2.043	1.878, 1.905 0.784
$AlT_{17}HT_{12}Cu^+8MR$ +H_2	-1359.8925500040 -1361.0896255991	2.046, 2.155 2.032, 2.136	1.653, 1.665 0.816
$AlT_{18}T_{12}Cu^{2+}6MR$ +H_2	-1359.3025412165 -1360.4769656265	1.961,1.965,2.097,2.204 1.969,1.971,2.102,2.232	2.430, 2.430 0.758
$AlT_{27}T_{12}Cu^{2+}6MR$ +H_2	-1359.3246746564 -1360.4979251239	1.990,1.991,2.052,2.053 1.996,1.996,2.062,2.062	2.524, 2.525 0.756
$AlT_{29}T_{12}Cu^{2+}4MR$ +H_2	-1359.2697771764 -1360.4502281315	1.990,2.030,2.142,2.152 2.037,2.047,2.066,2.297	1.967, 1.959 0.773
$AlT_{29}T_{12}Cu^{2+}6MR$ +H_2	-1359.2684615035 -1360.4427389242	1.946,2.072,2.158,2.159 1.952,2.080,2.175,2.180	2.418, 2.445 0.766
$AlT_{29}T_{12}Cu^{2+}8MR$ +H_2	-1359.2509481723 -1360.4431609093	2.038, 2.045, 2.134 2.037, 2.071	1.674, 1.682 0.808
$AlT_{30}T_{12}Cu^{2+}6MR$ +H_2	-1359.2811283908 -1360.4554652001	1.965,2.065,2.097,2.131 1.970,2.077,2.103,2.148	2.435, 2.427 0.758
$AlT_{33}T_{12}Cu^{2+}6MR$ +H_2	-1359.2775301795 -1360.4516311966	1.960,2.030,2.056,2.244 1.966,2.039,2.059,2.270	1.975, 1.992 0.774
$AlT_{33}T_{12}Cu^{2+}4MR$ +H_2	-1359.2703714552 -1360.4507088060	1.967,1.970,2.052,2.120 1.992,1.995,2.074,2.171	2.442, 2.427, 0.757
$AlT_{34}T_{12}Cu^{2+}8MR$ +H_2	-1359.2492235038 -1360.4419906470	2.051, 2.105, 2.172 2.065, 2.070	1.677, 1.667 0.810
H_2 molecule	-1.1665290485323	-	0.75

Table S2. Geometrical parameters of the Cu-H_2 complexes, binding energies, along with the dispersive(D3) contribution, and atomic magnetic moment of Cu, μ_{Cu},, in the as described environment."-" stands for non-polarised calculation. Dihydrogen rotational barrier and the corresponding computed tunneling frequency to be compared to the observed INS transitions.

Structure	E_b, kJ/mol H_2 (D3, kJ/mol H_2)	Rot. Barrier V_2, meV	μ_{Cu}, Bohr magneton	Tunnel Freq. Ω_t, cm^{-1}
$AlT_{12}Cu^+4MR$ +H_2	68.7 (6.7)	68.4	- -	3
$AlT_{12}Cu^+6MR$ +H_2	33.9 (4.1)	63.0	- -	24
$AlT_{12}Cu^+8MR$ +H_2	79.8 (9.5)	103.4	- -	0.86
$AlT_{29}Cu^+4MR$ +H_2	76.4 (8.0)	117.1	- -	0.56
$AlT_{30}HT_{12}Cu^+6MR$ +H_2	30.7 (4.7)	55.06	- -	5
$AlT_{30}HT_{12}Cu^+8MR$ +H_2	77.6 (9.5)	118.8	- -	0.55
$AlT_{30}T_{12}Cu^{2+}8MR$ +H2	75.2 (8.8)	107.7	0.197 0.000	0.81
$AlT_4T_{12}Cu^{2+}8MR$ +H_2	77.4 (8.9)	101.1	0.128 0.001	0.98
$AlT_4HT_{12}Cu^{2+}8MR$ +H_2	82.0 (11.6)	123.6	- -	0.44
$AlT_{17}T_{12}Cu^{2+}8MR$ +H_2	57.0 (9.8)	80.6	0.576 0.666	2.44
$AlT_{17}HT_{12}Cu^+8MR$ +H_2	80.2 (9.9)	136.9	0.000 0.000	0.31
$AlT_{18}T_{12}Cu^{2+}6MR$ +H_2	20.7 (11.9)	12.05	0.760 0.766	36
$AlT_{27}T_{12}Cu^{2+}6MR$ +H_2	17.6 (11.5)	5.90	0.796 0.802	46
$AlT_{29}T_{12}Cu^{2+}4MR$ +H_2	36.6 (3.1)	17.60	0.694 0.705	27
$AlT_{29}T_{12}Cu^{2+}6MR$ +H_2	20.4 (11.4)	5.80	0.640 0.650	46
$AlT_{29}T_{12}Cu^{2+}8MR$ +H_2	67.4 (10.0)	91.08	0.383 0.000	1.37
$AlT_{30}T_{12}Cu^{2+}6MR$ +H_2	20.5 (11.6)	10.0	0.704 0.712	39
$AlT_{33}T_{12}Cu^{2+}4MR$ +H_2	36.3 (11.1)	39.2	0.672 0.676	6.2
$AlT_{33}T_{12}Cu^{2+}6MR$ +H_2	19.9 (11.0)	4.07	0.691 0.694	49
$AlT_{34}T_{12}Cu^{2+}8MR$ +H_2	68.9 (5.4)	90.2	0.286 0.000	1.38

DFT relaxed structures in CIF-format

1. **The starting fully optimised CHA structure:**

data_CHA_P1
_symmetry_space_group_name_H-M   'P1'
_symmetry_Int_Tables_number   1
_symmetry_cell_setting   triclinic
loop_
_symmetry_equiv_pos_as_xyz
 x,y,z
_cell_length_a   13.6727
_cell_length_b   13.6727
_cell_length_c   14.7868
_cell_angle_alpha   89.9999
_cell_angle_beta   90.0000
_cell_angle_gamma   120.0000
loop_
_atom_site_label
_atom_site_type_symbol
_atom_site_fract_x
_atom_site_fract_y
_atom_site_fract_z
Si1 Si 1.00019 0.22758 0.10532
Si2 Si 0.66686 0.5609 0.43874
Si3 Si 0.33354 0.89421 0.77199
Si4 Si 0.77242 0.77262 0.10532
Si5 Si 0.4391 0.10595 0.43874
Si6 Si 0.1058 0.43934 0.77199
Si7 Si 0.22738 -1.92868E-4 0.10532
Si8 Si 0.89405 0.33314 0.43874
Si9 Si 0.56066 0.66646 0.77199
Si10 Si 0.22758 1.00019 0.89468
Si11 Si 0.89421 0.33354 0.22801

Si12 Al 0.5609 0.66686 0.56126

Si13 Si 0.77262 0.77242 0.89468

Si14 Si 0.43934 0.1058 0.22801

Si15 Si 0.10595 0.4391 0.56126

Si16 Si -1.9289E-4 0.22738 0.89468

Si17 Si 0.66646 0.56066 0.22801

Si18 Si 0.33314 0.89405 0.56126

Si19 Si -1.92783E-4 0.77242 0.89468

Si20 Si 0.66646 0.10579 0.22801

Si21 Si 0.33314 0.4391 0.56126

Si22 Si 0.22758 0.22738 0.89468

Si23 Si 0.8942 0.56066 0.22801

Si24 Si 0.5609 0.89405 0.56126

Si25 Si 0.77262 1.00019 0.89468

Si26 Si 0.43934 0.33354 0.22801

Si27 Si 0.10595 0.66686 0.56126

Si28 Si 0.77242 -1.92773E-4 0.10532

Si29 Si 0.4391 0.33314 0.43874

Si30 Si 0.10579 0.66646 0.77199

Si31 Si 0.22738 0.22758 0.10532

Si32 Si 0.89405 0.5609 0.43874

Si33 Al 0.56066 0.8942 0.77199

Si34 Si 1.00019 0.77262 0.10532

Si35 Si 0.66686 0.10595 0.43874

Si36 Si 0.33354 0.43934 0.77199

O37 O 0.90218 0.09782 0.12324

O38 O 0.56874 0.43126 0.45691

O39 O 0.23554 0.76446 0.79

O40 O 0.90218 0.80437 0.12324

O41 O 0.56874 0.13748 0.45691

O42 O 0.23554 0.47107 0.79

O43 O 0.19563 0.09782 0.12324

O44 O 0.86252 0.43126 0.45691

O45 O 0.52893 0.76446 0.79

O46 O 0.09782 0.90218 0.87676

O47 O 0.76446 0.23554 0.21

O48 O 0.43126 0.56874 0.54309

O49 O 0.80437 0.90218 0.87676

O50 O 0.47107 0.23554 0.21

O51 O 0.13748 0.56874 0.54309

O52 O 0.09782 0.19563 0.87676

O53 O 0.76446 0.52893 0.21

O54 O 0.43126 0.86252 0.54309

O55 O 0.98012 0.3134 0.16675

O56 O 0.64701 0.64701 0.5

O57 O 0.6866 0.66672 0.16675

O58 O 0.35299 9.59275E-8 0.5

O59 O 0.33328 0.01988 0.16675

O60 O 1.04792E-7 0.35299 0.5

O61 O 0.3134 0.98012 0.83325

O62 O 0.66672 0.6866 0.83325

O63 O 0.01988 0.33328 0.83325

O64 O 0.01988 0.6866 0.83325

O65 O 0.3134 0.33328 0.83325

O66 O 0.66672 0.98012 0.83325

O67 O 0.6866 0.01988 0.16675

O68 O 0.35299 0.35299 0.5

O69 O 0.33328 0.3134 0.16675

O70 O -1.00566E-7 0.64701 0.5

O71 O 0.98012 0.66672 0.16675

O72 O 0.64701 -1.11647E-7 0.5

O73 O 0.12037 0.24075 0.13282

O74 O 0.78698 0.57397 0.46625

O75 O 0.45372 0.90744 0.79961

O76 O 0.75925 0.87963 0.13282

O77 O 0.42603 0.21302 0.46625

O78 O 0.09256 0.54628 0.79961

O79 O 0.12037 0.87963 0.13282

O80 O 0.78698 0.21302 0.46625

O81 O 0.45372 0.54628 0.79961

O82 O 0.24075 0.12037 0.86718

O83 O 0.90744 0.45372 0.20039

O84 O 0.57397 0.78698 0.53375

O85 O 0.87963 0.75925 0.86718

O86 O 0.54628 0.09256 0.20039

O87 O 0.21302 0.42603 0.53375

O88 O 0.87963 0.12037 0.86718

O89 O 0.54628 0.45372 0.20039

O90 O 0.21302 0.78698 0.53375

O91 O -1.91685E-7 0.26028 4.23299E-8

O92 O 0.66659 0.59334 0.33337

O93 O 0.33341 0.92675 0.66663

O94 O 0.73972 0.73972 9.23521E-9

O95 O 0.40666 0.07325 0.33337

O96 O 0.07325 0.40666 0.66663

O97 O 0.26028 -1.63419E-7 -4.63801E-8

O98 O 0.92675 0.33341 0.33337

O99 O 0.59333 0.66659 0.66663

O100 O 1.9357E-7 0.73972 -3.98949E-8

O101 O 0.66659 0.07325 0.33337

O102 O 0.33341 0.40666 0.66663

O103 O 0.26028 0.26028 -1.81167E-9

O104 O 0.92675 0.59334 0.33337

O105 O 0.59334 0.92675 0.66663

O106 O 0.73972 1.84575E-7 4.69034E-8

O107 O 0.40666 0.33341 0.33337

O108 O 0.07325 0.66659 0.66663

2. **Relaxed(unit cell angles kept fixed) CHA structure with an Al -atom in T12, Cu-centre(Cu-H$_2$ complex) in the 8MR**

data_CHA_P1_AlT12-Cu8MR + H2

_symmetry_space_group_name_H-M   'P1'

_symmetry_Int_Tables_number   1

_symmetry_cell_setting   triclinic

loop_

_symmetry_equiv_pos_as_xyz

 x,y,z

_cell_length_a   13.6833

_cell_length_b   13.6833

_cell_length_c   14.7983

_cell_angle_alpha   89.999993

_cell_angle_beta   90.0000066

_cell_angle_gamma   120.000007

loop_

_atom_site_label

_atom_site_type_symbol

_atom_site_fract_x

_atom_site_fract_y

_atom_site_fract_z

Si1 Si 1.00227 0.22752 0.1075

Si2 Si 0.66929 0.56146 0.43788

Si3 Si 0.33361 0.89329 0.77393

Si4 Si 0.77891 0.77501 0.11124

Si5 Si 0.43521 0.10523 0.43822

Si6 Si 0.10496 0.43881 0.7752

Si7 Si 0.22979 -0.00101 0.10619

Si8 Si 0.89558 0.33561 0.4395

Si9 Si 0.56235 0.66495 0.77755

Si10 Si 0.2268 0.99979 0.89471

Si11 Si 0.89761 0.33225 0.23199

Si12 Al 0.56098 0.66601 0.56673

Si13 Si 0.77297 0.77188 0.89796

Si14 Si 0.43922 0.10413 0.23063

Si15 Si 0.10404 0.43729 0.56477

Si16 Si -2.97998E-4 0.2264 0.89725

Si17 Si 0.66913 0.55654 0.22355

Si18 Si 0.33427 0.89614 0.56347

Si19 Si -0.00109 0.77288 0.89471

Si20 Si 0.6688 0.10405 0.23306

Si21 Si 0.32867 0.4348 0.5639

Si22 Si 0.22677 0.22604 0.89655

Si23 Si 0.8972 0.56126 0.22705

Si24 Si 0.56308 0.8988 0.56424

Si25 Si 0.77137 0.99765 0.89721

Si26 Si 0.4422 0.33419 0.22867

Si27 Si 0.10715 0.66612 0.5627

Si28 Si 0.77388 -0.00149 0.10868

Si29 Si 0.44008 0.33687 0.44085

Si30 Si 0.10465 0.6651 0.77338

Si31 Si 0.22775 0.22475 0.1082

Si32 Si 0.8968 0.56539 0.43759

Si33 Si 0.55906 0.89022 0.77706

Si34 Si 1.00375 0.77219 0.10748

Si35 Si 0.6667 0.10885 0.44084

Si36 Si 0.3319 0.43706 0.77303

O37 O 0.90253 0.09855 0.12547

O38 O 0.56818 0.43624 0.46478

O39 O 0.23422 0.76389 0.78985

O40 O 0.90654 0.80287 0.13375

O41 O 0.56534 0.1362 0.45148

O42 O 0.23419 0.46943 0.79203

O43 O 0.1971 0.09557 0.1277

O44 O 0.86667 0.43597 0.45114

O45 O 0.52923 0.76246 0.79858

O46 O 0.09721 0.90218 0.87606

O47 O 0.76744 0.23346 0.2158

O48 O 0.42332 0.56289 0.54778

O49 O 0.80264 0.90022 0.87565

O50 O 0.47205 0.23429 0.21437

O51 O 0.13779 0.56748 0.54425

O52 O 0.09676 0.19369 0.87862

O53 O 0.76891 0.52895 0.20145

O54 O 0.43449 0.86848 0.54297

O55 O 0.98257 0.31377 0.16847

O56 O 0.6536 0.65941 0.48518

O57 O 0.68857 0.6676 0.16948

O58 O 0.35153 0.00211 0.50301

O59 O 0.33893 0.02042 0.16388

O60 O -0.0046 0.35191 0.50566

O61 O 0.31317 0.97916 0.83483

O62 O 0.66015 0.67997 0.84784

O63 O 0.01879 0.33194 0.83599

O64 O 0.01956 0.68633 0.83487

O65 O 0.31279 0.33363 0.83765

O66 O 0.66543 0.97986 0.83701

O67 O 0.68732 0.01797 0.17026

O68 O 0.3486 0.3489 0.50067

O69 O 0.33405 0.3112 0.16903

O70 O 0.0038 0.64938 0.49884

O71 O 0.98619 0.66378 0.1643

O72 O 0.65156 0.01096 0.50935

O73 O 0.12076 0.23778 0.13626

O74 O 0.78878 0.57495 0.46879

O75 O 0.4522 0.90448 0.80327

O76 O 0.7653 0.88144 0.1416

O77 O 0.42762 0.21561 0.46361

O78 O 0.09209 0.54596 0.80342

O79 O 0.12479 0.87795 0.13472

O80 O 0.78402 0.21926 0.46583

O81 O 0.4519 0.54404 0.79906

O82 O 0.24051 0.11994 0.86706

O83 O 0.90995 0.45246 0.2071

O84 O 0.58231 0.79848 0.52754

O85 O 0.87864 0.75846 0.86612

O86 O 0.54857 0.09222 0.209

O87 O 0.20562 0.41663 0.53693

O88 O 0.87832 0.11917 0.87272

O89 O 0.5491 0.4511 0.1941

O90 O 0.21507 0.78689 0.53747

O91 O 0.00302 0.26077 0.00259

O92 O 0.66961 0.58239 0.33003

O93 O 0.33618 0.92833 0.66892

O94 O 0.75235 0.74863 0.00552

O95 O 0.39768 0.06765 0.3341

O96 O 0.07065 0.4077 0.67017

O97 O 0.25857 -2.69763E-4 1.79974E-4

O98 O 0.93269 0.33074 0.33627

O99 O 0.60596 0.67374 0.67633

O100 O -0.00152 0.74338 9.58767E-4

O101 O 0.67066 0.06797 0.33787

O102 O 0.32602 0.39739 0.6691

O103 O 0.25818 0.25523 0.00259

O104 O 0.92483 0.60041 0.3319

O105 O 0.58983 0.92038 0.67103

O106 O 0.73907 -0.00727 0.00365

O107 O 0.41608 0.34359 0.33405

O108 O 0.07145 0.66327 0.66771

Cu Cu 0.6791 0.804 0.41882

H1 H 0.72295 0.90366 0.34152

H2 H 0.74487 0.86182 0.323

3. **Relaxed(unit cell angles only kept fixed) CHA structure with an Al -atom in T12 Cu-centre(Cu-H2 complex) in the 6MR.**

data_CHA_P1_AlT12-Cu6MR

_symmetry_space_group_name_H-M   'P1'

_symmetry_Int_Tables_number   1

_symmetry_cell_setting   triclinic

loop_

_symmetry_equiv_pos_as_xyz

 x,y,z

_cell_length_a   13.6909

_cell_length_b   13.6909

_cell_length_c   14.8065

_cell_angle_alpha   89.999993

_cell_angle_beta   90.0000066

_cell_angle_gamma   120.000007

loop_

_atom_site_label

_atom_site_type_symbol

_atom_site_fract_x

_atom_site_fract_y

_atom_site_fract_z

Si1 Si 1.00299 0.22746 0.10639

Si2 Si 0.6712 0.56075 0.43782

Si3 Si 0.33275 0.89587 0.77275

Si4 Si 0.77822 0.77481 0.10991

Si5 Si 0.43608 0.10508 0.43778

Si6 Si 0.10451 0.43978 0.77437

Si7 Si 0.22915 2.43634E-4 0.10633

Si8 Si 0.89612 0.33343 0.43759

Si9 Si 0.55981 0.66788 0.78002

Si10 Si 0.22782 1.00154 0.89508

Si11 Si 0.89782 0.33251 0.23016

Si12 Al 0.56597 0.66944 0.56429

Si13 Si 0.77401 0.7744 0.89699

Si14 Si 0.44054 0.10439 0.22914

Si15 Si 0.104 0.43597 0.56446

Si16 Si 9.7016E-5 0.22706 0.89614

Si17 Si 0.67038 0.55877 0.22585

Si18 Si 0.33049 0.89952 0.56445

Si19 Si -2.6586E-4 0.77461 0.89344

Si20 Si 0.66778 0.10532 0.23093

17

Si21 Si 0.332 0.43754 0.56295

Si22 Si 0.2265 0.22664 0.89448

Si23 Si 0.8995 0.56186 0.22658

Si24 Si 0.56249 0.89909 0.56428

Si25 Si 0.77135 0.99997 0.89725

Si26 Si 0.44212 0.33538 0.22807

Si27 Si 0.10955 0.66494 0.56184

Si28 Si 0.77454 -8.77994E-4 0.10841

Si29 Si 0.44245 0.33723 0.43717

Si30 Si 0.107 0.66673 0.77353

Si31 Si 0.2288 0.22672 0.10644

Si32 Si 0.89957 0.56336 0.4355

Si33 Si 0.56143 0.89355 0.77543

Si34 Si 1.00323 0.77266 0.10581

Si35 Si 0.66515 0.10797 0.44083

Si36 Si 0.33481 0.44112 0.77374

O37 O 0.90419 0.0983 0.12381

O38 O 0.57319 0.4296 0.45622

O39 O 0.23647 0.76556 0.79072

O40 O 0.9064 0.80353 0.13124

O41 O 0.56493 0.1363 0.45913

O42 O 0.23385 0.4696 0.78755

O43 O 0.19752 0.09764 0.12704

O44 O 0.86773 0.43361 0.45045

O45 O 0.52821 0.76614 0.80228

O46 O 0.09877 0.90374 0.87563

O47 O 0.76752 0.23464 0.21521

O48 O 0.42014 0.5691 0.53993

O49 O 0.80275 0.90266 0.87572

O50 O 0.46995 0.23382 0.21651

O51 O 0.14422 0.56827 0.54231

O52 O 0.09665 0.19408 0.87594

O53 O 0.77053 0.53039 0.20667

O54 O 0.43412 0.87571 0.54946

O55 O 0.98232 0.3134 0.16673

O56 O 0.65365 0.6473 0.49618

O57 O 0.68885 0.66585 0.16661

O58 O 0.34717 0.00232 0.50098

O59 O 0.33684 0.02031 0.16526

O60 O -0.00216 0.35186 0.50319

O61 O 0.31534 0.98067 0.8371

O62 O 0.66218 0.68388 0.84499

O63 O 0.01957 0.33322 0.83534

O64 O 0.02077 0.68892 0.83235

O65 O 0.31177 0.33354 0.83427

O66 O 0.66564 0.98315 0.83694

O67 O 0.6894 0.01997 0.17033

O68 O 0.35716 0.35546 0.50113

O69 O 0.33686 0.31398 0.16516

O70 O 0.00545 0.64543 0.49894

O71 O 0.98595 0.66424 0.16241

O72 O 0.65055 0.00806 0.50698

O73 O 0.12254 0.24038 0.13547

O74 O 0.79204 0.57333 0.46341

O75 O 0.45464 0.91067 0.79387

O76 O 0.76412 0.88097 0.13881

O77 O 0.42294 0.21307 0.45882

O78 O 0.09377 0.54756 0.80438

O79 O 0.12403 0.87881 0.13331

O80 O 0.78523 0.21663 0.46399

O81 O 0.45085 0.54776 0.807

O82 O 0.24135 0.12109 0.86571

O83 O 0.91103 0.45275 0.20405

O84 O 0.55773 0.78734 0.52441

O85 O 0.88016 0.76172 0.86486

O86 O 0.54939 0.09468 0.20089

O87 O 0.20618 0.41401 0.53982

O88 O 0.87838 0.12099 0.8716

O89 O 0.55137 0.45128 0.19611

O90 O 0.21693 0.78549 0.53469

O91 O 0.0048 0.26128 0.00143

O92 O 0.66905 0.58763 0.33099

O93 O 0.32445 0.92973 0.66893

O94 O 0.75216 0.74851 0.00383

O95 O 0.40579 0.06533 0.33333

O96 O 0.06789 0.40937 0.66935

O97 O 0.25933 0.0025 5.18351E-4

O98 O 0.93413 0.33115 0.33428

O99 O 0.59451 0.67286 0.67709

O100 O -7.39881E-4 0.74375 -7.43581E-4

O101 O 0.66199 0.07008 0.33643

O102 O 0.34099 0.41122 0.66842

O103 O 0.25741 0.25621 3.86263E-4

O104 O 0.9345 0.59992 0.3309

O105 O 0.59761 0.91999 0.66971

O106 O 0.73947 -0.00403 0.00341

O107 O 0.41053 0.34396 0.33233

O108 O 0.07639 0.66287 0.66698

Cu Cu 0.39541 0.68023 0.46493

H1 H 0.29737 0.6521 0.38666

H2 H 0.33962 0.71932 0.38201

4. **Relaxed(unit cell angles only kept fixed) CHA structure with an Al -atom in T12, T4, Cu-centre(Cu-H2 complex) in the 8MR.**

data_CHA_P1_AlT4AlT12-Cu+H2-8MR

_symmetry_space_group_name_H-M   'P1'

_symmetry_Int_Tables_number   1

_symmetry_cell_setting   triclinic

loop_

_symmetry_equiv_pos_as_xyz

 x,y,z

_cell_length_a   13.7022

_cell_length_b   13.7022

_cell_length_c   14.8187

_cell_angle_alpha   89.999993

_cell_angle_beta   90.000006

_cell_angle_gamma   120.000007

loop_

_atom_site_label

_atom_site_type_symbol

_atom_site_fract_x

_atom_site_fract_y

_atom_site_fract_z

Si1 Si 1.002 0.22934 0.10752

Si2 Si 0.66667 0.55209 0.44231

Si3 Si 0.33625 0.89419 0.77386

Si4 Al 0.77475 0.77582 0.11433

Si5 Si 0.43406 0.10192 0.43763

Si6 Si 0.1079 0.44151 0.7775

Si7 Si 0.23422 1.57732E-4 0.10563

Si8 Si 0.89604 0.33472 0.44028

Si9 Si 0.56479 0.66601 0.77415

Si10 Si 0.23141 1.00243 0.89494

Si11 Si 0.9045 0.33765 0.23495

Si12 Al 0.55695 0.66293 0.56108

Si13 Si 0.77415 0.77229 0.8974

Si14 Si 0.4375 0.10391 0.23302

Si15 Si 0.10315 0.43652 0.56645

Si16 Si 0.00219 0.22805 0.89826

Si17 Si 0.66837 0.54959 0.22569

Si18 Si 0.33384 0.89461 0.56316

Si19 Si 0.00283 0.77453 0.8968

Si20 Si 0.67169 0.11432 0.23122

Si21 Si 0.32563 0.43091 0.56477

Si22 Si 0.22984 0.22764 0.89859

Si23 Si 0.89839 0.56405 0.22967

Si24 Si 0.56303 0.89696 0.55992

Si25 Si 0.77378 0.99946 0.8955

Si26 Si 0.43804 0.33561 0.23285

Si27 Si 0.10812 0.66505 0.56287

Si28 Si 0.76996 0.00296 0.1072

Si29 Si 0.43744 0.33482 0.44361

Si30 Si 0.10795 0.66707 0.77475

Si31 Si 0.22796 0.22431 0.10981

Si32 Si 0.89487 0.56442 0.44011

Si33 Si 0.56313 0.89196 0.77324

Si34 Si 1.00703 0.77469 0.10776

Si35 Si 0.66633 0.10889 0.43843

Si36 Si 0.33414 0.43935 0.77533

O37 O 0.89892 0.10326 0.12458

O38 O 0.56379 0.4309 0.47565

O39 O 0.23744 0.76534 0.79238

O40 O 0.91498 0.8103 0.12978

O41 O 0.56469 0.13535 0.45236

O42 O 0.23726 0.47248 0.79439

O43 O 0.20173 0.09655 0.129

O44 O 0.86742 0.43541 0.44884

O45 O 0.53353 0.76439 0.79588

O46 O 0.10218 0.90364 0.87848

O47 O 0.77313 0.24321 0.21868

O48 O 0.41964 0.55814 0.54347

O49 O 0.80381 0.90121 0.87499

O50 O 0.4592 0.23031 0.22379

O51 O 0.13853 0.56639 0.54342

O52 O 0.10022 0.19635 0.88138

O53 O 0.76945 0.52397 0.19993

O54 O 0.43434 0.86779 0.54185

O55 O 0.98736 0.31827 0.16951

O56 O 0.64909 0.65425 0.48004

O57 O 0.68673 0.66426 0.1839

O58 O 0.35122 0.00168 0.5047

O59 O 0.34274 0.02016 0.16319

O60 O -0.00783 0.3505 0.51044

O61 O 0.31714 0.98138 0.83417

O62 O 0.66894 0.68343 0.83663

O63 O 0.02204 0.33355 0.83671

O64 O 0.02207 0.68933 0.83363

O65 O 0.31516 0.33602 0.83969

O66 O 0.67028 0.98228 0.83166

O67 O 0.68481 0.03109 0.16254

O68 O 0.34402 0.34167 0.5052

O69 O 0.32967 0.31299 0.17355

O70 O 0.0028 0.64688 0.50122

O71 O 0.98753 0.66723 0.16793

O72 O 0.65066 0.00799 0.50385

O73 O 0.1181 0.23345 0.13452

O74 O 0.78641 0.56991 0.47764

O75 O 0.45632 0.90627 0.79949

O76 O 0.75582 0.88786 0.14491

O77 O 0.42373 0.21178 0.45793

O78 O 0.09482 0.54816 0.80621

O79 O 0.13181 0.87768 0.13208

O80 O 0.78328 0.2187 0.46502

O81 O 0.45514 0.54607 0.79976

O82 O 0.24332 0.12198 0.86707

O83 O 0.92096 0.46031 0.21454

O84 O 0.57917 0.79507 0.52158

O85 O 0.88374 0.76293 0.86921

O86 O 0.55385 0.10773 0.2095

O87 O 0.20246 0.41225 0.53861

O88 O 0.88225 0.12056 0.87167

O89 O 0.54825 0.44503 0.19353

O90 O 0.21531 0.78544 0.53603

O91 O 0.00414 0.26403 0.00275

O92 O 0.6667 0.5588 0.33452

O93 O 0.33484 0.92547 0.66858

O94 O 0.74276 0.74274 0.00106

O95 O 0.39663 0.05801 0.33492

O96 O 0.07394 0.41147 0.67253

O97 O 0.26569 0.00538 -1.95942E-4

O98 O 0.93812 0.33014 0.33885

O99 O 0.5997 0.66972 0.67081

O100 O 0.00424 0.74141 0.00155

O101 O 0.67079 0.07181 0.33457

O102 O 0.32742 0.40059 0.67106

O103 O 0.26183 0.25583 0.00456

O104 O 0.91887 0.6035 0.33517

O105 O 0.59208 0.91818 0.66644

O106 O 0.73943 -0.00249 4.61684E-4

O107 O 0.41751 0.35343 0.33823

O108 O 0.07661 0.6637 0.66858

Cu Cu 0.66589 0.78705 0.40606

H1 H 0.69281 0.88949 0.33234

H2 H 0.70751 0.84934 0.30228

5. **Relaxed(unit cell angles only kept fixed) CHA structure with an Al -atom in T12 and T27, Cu-centre(Cu-H2 complex) in the 6MR.**

data_CHA_P1_AlT27T12-Cu+H2-6MR

_symmetry_space_group_name_H-M   'P1'

_symmetry_Int_Tables_number   1

_symmetry_cell_setting   triclinic

loop_

_symmetry_equiv_pos_as_xyz

 x,y,z

_cell_length_a   13.6445

_cell_length_b   13.6445

_cell_length_c   14.7563

_cell_angle_alpha   89.999993

_cell_angle_beta   90.00006

_cell_angle_gamma   120.000007

loop_

_atom_site_label

_atom_site_type_symbol

_atom_site_fract_x

_atom_site_fract_y

_atom_site_fract_z

Si1 Si 0.99975 0.22619 0.10924

Si2 Si 0.67396 0.57111 0.43536

Si3 Si 0.33035 0.89423 0.77278

Si4 Si 0.7735 0.77237 0.10363

Si5 Si 0.43492 0.1025 0.44024

Si6 Si 0.10741 0.44234 0.77374

Si7 Si 0.22771 -0.00166 0.10774

Si8 Si 0.88683 0.33847 0.44074

Si9 Si 0.55912 0.66732 0.77551

Si10 Si 0.2343 1.00361 0.89504

Si11 Si 0.89274 0.33209 0.22928

Si12 Al 0.54387 0.66498 0.55742

Si13 Si 0.77595 0.7778 0.89029

Si14 Si 0.43738 0.10345 0.23055

Si15 Si 0.10364 0.42621 0.56532

Si16 Si 4.49068E-4 0.2255 0.89899

Si17 Si 0.66817 0.55937 0.22173

Si18 Si 0.34096 0.90863 0.57067

Si19 Si 0.00367 0.77771 0.89016

Si20 Si 0.66811 0.10351 0.23056

Si21 Si 0.32454 0.42616 0.56536

Si22 Si 0.22676 0.22533 0.89892

Si23 Si 0.89306 0.55934 0.2217

Si24 Si 0.56959 0.90862 0.57063

Si25 Si 0.77104 1.00363 0.89521

Si26 Si 0.44128 0.33219 0.22929

Si27 Al 0.12308 0.66497 0.55739

Si28 Si 0.7725 -0.00162 0.10772

Si29 Si 0.45354 0.3385 0.44065

Si30 Si 0.10998 0.66725 0.7755

Si31 Si 0.22823 0.22591 0.10929

Si32 Si 0.8992 0.57123 0.43529

Si33 Si 0.56564 0.89417 0.77276

Si34 Si 1.00093 0.77229 0.10356

Si35 Si 0.66966 0.10268 0.44037

Si36 Si 0.33685 0.4423 0.77379

O37 O 0.90134 0.09688 0.12898

O38 O 0.58375 0.43663 0.45452

O39 O 0.23861 0.76631 0.8027

O40 O 0.90163 0.80112 0.12631

O41 O 0.55908 0.1162 0.45418

O42 O 0.24029 0.47863 0.77668

O43 O 0.19712 0.0966 0.12937

O44 O 0.85498 0.43677 0.45445

O45 O 0.52926 0.76619 0.80267

O46 O 0.10684 0.90517 0.87041

O47 O 0.76389 0.23295 0.20784

O48 O 0.39358 0.56304 0.54057

O49 O 0.80042 0.90538 0.87075

O50 O 0.47106 0.23301 0.20829

O51 O 0.17151 0.56309 0.5406

O52 O 0.09326 0.18478 0.88698

O53 O 0.76467 0.52749 0.19655

O54 O 0.4695 0.93707 0.57865

O55 O 0.98274 0.31258 0.1728

O56 O 0.63348 0.64864 0.48576

O57 O 0.68236 0.66319 0.1597

O58 O 0.33864 -0.00138 0.50078

O59 O 0.33478 0.01589 0.16699

O60 O -0.00527 0.36095 0.50168

O61 O 0.32698 0.98601 0.83994

O62 O 0.66986 0.68728 0.83134

O63 O 0.03247 0.33443 0.83711

O64 O 0.01896 0.68701 0.8312

O65 O 0.30381 0.33445 0.83725

O66 O 0.66088 0.98593 0.83987

O67 O 0.68301 0.01564 0.16727

O68 O 0.36816 0.3608 0.50181

O69 O 0.3318 0.31243 0.17265

O70 O 0.01725 0.64877 0.48563

O71 O 0.98266 0.66293 0.15948

O72 O 0.66193 -0.00135 0.50078

O73 O 0.12036 0.23878 0.1342

O74 O 0.79878 0.59558 0.467

O75 O 0.45581 0.90983 0.77475

O76 O 0.75965 0.8782 0.13468

O77 O 0.43984 0.2183 0.4712

O78 O 0.09458 0.54682 0.80919

O79 O 0.1207 0.87795 0.13474

O80 O 0.78039 0.21843 0.4717

O81 O 0.45421 0.54677 0.80915

O82 O 0.24797 0.12431 0.86684

O83 O 0.9074 0.45167 0.19859

O84 O 0.5104 0.77661 0.53378

O85 O 0.88651 0.77119 0.86146

O86 O 0.54498 0.08795 0.21137

O87 O 0.19113 0.38026 0.54746

O88 O 0.87805 0.12447 0.86727

O89 O 0.54617 0.45173 0.19844

O90 O 0.26819 0.77661 0.53387

O91 O -0.00351 0.25851 0.00398

O92 O 0.67648 0.59418 0.32695

O93 O 0.29888 0.91856 0.67085

O94 O 0.74783 0.74765 -0.00334

O95 O 0.39708 0.07366 0.33532

O96 O 0.06253 0.40893 0.66973

O97 O 0.25931 0.00152 0.00188

O98 O 0.91966 0.33235 0.33623

O99 O 0.57856 0.66719 0.66905

O100 O 0.00194 0.74779 -0.00346

O101 O 0.67906 0.07431 0.33541

O102 O 0.34831 0.40885 0.66978

O103 O 0.26372 0.25782 0.00396

O104 O 0.91963 0.59438 0.32687

O105 O 0.62148 0.91847 0.67084

O106 O 0.74345 0.0013 0.00198

O107 O 0.41456 0.3329 0.33619

O108 O 0.09053 0.66702 0.66901

Cu Cu 0.33716 0.67231 0.53041

H1 H 0.31501 0.68441 0.36167

H2 H 0.369 0.6817 0.36132

Coordinates of the atoms in the 23 tetrahedrals cluster structure:

(lines in bold fond indicate the atoms/coordinates which were optimized, the rest stay fixed)

H	4.75898800	-0.01233200	6.92510500
H	5.66027700	0.45018300	-4.98824300
H	-2.77639600	4.08134900	5.35276900
H	-2.23494100	-4.51010600	5.18502900
H	1.59205300	4.51263000	-5.76540600
H	-2.32347800	6.60086200	-1.78460100

H	-3.32258200	6.49566400	2.64454400
H	-6.73093000	3.79825800	1.81411700
H	2.13340800	-4.07885400	-5.93297000
H	-5.81666700	3.92390500	-2.58764900
H	-4.96227700	-4.48179400	-2.90681200
H	-6.12882400	-4.59566900	1.68475300
H	7.47923400	-2.17208700	0.17503100
H	8.26240100	1.79426900	0.89028900
H	-5.71845300	-0.15796900	-4.69870300
H	4.37503600	4.47977600	2.20324600
H	6.08783800	-3.79570900	-2.39432200
H	2.67958300	-6.49314500	-3.22474100
H	1.68038600	-6.59811300	1.20437000
H	7.36514000	1.70112900	4.43970300
H	6.45158600	-2.25224200	4.57334500
H	5.17276500	-3.92098900	2.00720200
H	-6.30326200	-0.44768500	4.40800200
H	0.86552900	6.65643200	0.99431300
H	1.70366000	6.80787800	-2.50562200
H	5.48603400	4.59835800	-2.26494300
H	-1.78960600	-6.58144800	-1.85977100
H	-2.60242000	-6.84465200	2.36812900
H	-8.74957600	1.82013400	-0.66412700
H	-8.83054800	-2.13152500	-0.85704900
O	5.66410000	0.46328300	-4.03213900
O	-1.96055200	5.72696400	-1.68437400
O	7.13340100	-1.28644100	0.15157700
O	3.67947400	3.85701500	2.00093900
O	7.74303000	1.21704600	0.33510100
O	0.66783300	5.76118100	1.26016000
O	4.32990300	-3.53544300	1.78321600
O	-2.93231900	5.63696300	2.48651400
O	6.16404300	-1.37542400	4.32304600
O	4.80439000	3.93246900	-2.29736300

O	6.61811300	1.14159200	4.63340500
O	1.65461900	5.94406000	-2.90625200
O	5.22499200	-3.39110800	-2.40536100
O	-0.90957400	3.99859800	2.36795700
O	-0.67531500	4.05771200	-0.22077100
O	-0.23912600	4.10766200	-2.77817600
O	1.13326500	4.39287200	-4.93231000
O	-2.32131000	4.05142400	4.51009400
O	4.68264500	0.05611500	5.97108900
O	1.67832500	-4.04892500	-5.09029800
Si	-4.70855500	-0.22906500	-2.45369000
Si	-3.93235800	2.62909000	-1.59205100
Si	-3.45961200	-2.89555900	-1.65878700
Si	-0.73222500	-4.28266700	-1.73428200
Si	-5.61437800	-0.33826800	2.02649000
Si	-4.58071400	2.53437700	1.49064900
Si	-4.20609700	-3.00023200	1.39530200
Si	-1.86245300	-4.49051400	2.75766600
Si	-2.39881300	4.20185000	2.91617400
O	-3.98911600	1.15591800	-2.18013500
O	-2.45382500	3.18617300	-1.87132700
O	1.31756400	-5.72446700	1.10417000
O	-4.32246200	-3.85452100	-2.58114400
O	-1.91726000	-3.22514300	-1.86919200
O	-4.97289000	3.53793800	-2.36341900
O	-1.31081800	-5.75868500	-1.84036400
O	-4.82031100	1.02564300	1.91695500
O	-3.32664100	3.07623800	2.30708400
O	2.28933400	-5.63447000	-3.06671800
O	-5.44737800	-3.92997300	1.71716100
O	-2.92378700	-3.43487600	2.23448500
O	-5.86797700	3.39360600	1.82515800
O	-2.29760800	-5.94156300	2.32605100
O	-4.26685300	2.63716100	-0.05570500

O	-3.87235300	-3.09283400	-0.13892300
O	-5.08787600	-0.33853700	-3.99986700
O	-6.00637700	-0.40544800	-1.56307000
O	-6.75458600	-0.41980100	0.92243900
O	0.26659100	-3.99610200	-2.94816200
O	0.03232800	-4.05521300	-0.35943100
O	-0.40385900	-4.10516400	2.19797500
O	-3.68890400	-1.37899200	-1.97325700
O	-4.55370900	-1.50592100	1.82547100
O	-6.30708600	-0.46079000	3.45193700
O	-1.77624900	-4.39037600	4.35210500
O	-8.03100100	1.19389400	-0.60903100
O	-8.24552500	-1.38895800	-0.75405400
Si	-1.33421200	4.28843900	-1.63224400
Si	-7.22919300	-0.17880300	-0.57883300
O	**3.11011200**	**-1.11502800**	**1.50038000**
O	**1.77660400**	**-3.16895100**	**1.41374900**
O	**4.17760200**	**-0.98850400**	**-2.35173500**
O	**2.71013200**	**-2.99851700**	**-2.99812300**
O	**3.48997500**	**-2.79484100**	**-0.54017600**
O	**3.08041700**	**3.35652300**	**-0.45489200**
O	**4.38115300**	**0.41956700**	**3.51085300**
O	**5.29782500**	**0.51683100**	**0.71554300**
O	**6.35910400**	**0.42381100**	**-1.67606300**
O	**2.79807700**	**1.37542700**	**1.35648500**
O	**3.93235600**	**1.49665200**	**-2.20688400**
O	**2.29473900**	**3.35101400**	**-2.91775600**
O	**1.20713900**	**3.20869700**	**1.37110800**
Si	**1.76368200**	**-4.19060100**	**-3.51896500**
Si	**0.69936400**	**-4.28747400**	**1.07301200**
Si	**3.24829400**	**-2.64049900**	**1.03982900**
Si	**6.61883600**	**0.19968300**	**-0.08757200**
Si	**2.75959400**	**2.95409100**	**1.06991500**
Si	**0.07525900**	**4.29945200**	**1.16294100**

Si	5.02022200	0.36325000	-2.58196800
Si	3.92864200	-2.53860900	-2.05911200
Si	5.47372900	0.04498400	4.59657800
Si	3.54549500	3.03314500	-1.95726200
Si	1.22106200	4.47007600	-3.35336500
Al	4.07798800	0.29394600	1.85832600
Cu	1.36630400	-0.02715800	1.21629200
H	-0.12168600	-0.68073900	1.01751100
H	-0.24918400	0.11420600	0.98491700

References

S1. M. J. Frisch, G. W. Trucks, H. B. Schlegel, G. E. Scuseria, M. A. Robb, J. R. Cheeseman, G. Scalmani, V. Barone, B. Mennucci, G. A. Petersson, H. Nakatsuji, M. Caricato, X. Li, H. P. Hratchian, A. F. Izmaylov, J. Bloino, G. Zheng, J. L. Sonnenberg, M. Hada, M. Ehara, K. Toyota, R. Fukuda, J. Hasegawa, M. Ishida, T. Nakajima, Y. Honda, O. Kitao, H. Nakai, T. Vreven, J. A. Montgomery, Jr., J. E. Peralta, F. Ogliaro, M. Bearpark, J. J. Heyd, E. Brothers, K. N. Kudin, V. N. Staroverov, R. Kobayashi, J. Normand, K. Raghavachari, A. Rendell, J. C. Burant, S. S. Iyengar, J. Tomasi, M. Cossi, N. Rega, J. M. Millam, M. Klene, J. E. Knox, J. B. Cross, V. Bakken, C. Adamo, J. Jaramillo, R. Gomperts, R. E. Stratmann, O. Yazyev, A. J. Austin, R. Cammi, C. Pomelli, J. W. Ochterski, R. L. Martin, K. Morokuma, V. G. Zakrzewski, G. A. Voth, P. Salvador, J. J. Dannenberg, S. Dapprich, A. D. Daniels, O. Farkas, J. B. Foresman, J. V. Ortiz, J. Cioslowski, and D. J. Fox, Gaussian, Inc., Wallingford CT, 2009.

S2. Becke, A. D.; J. Chem. Phys. **1993**, *98*, 5648; C. Lee, W. Yang, and R. G. Parr *Phys. Rev. B* **1988**, *37*, 785.

S3. H. v. Koningsveld, H. v.Bekkum, J.C. Jansen, Acta Cryst. B, 43 (1987) 127-132.

S4. Turner, S.; Sieber, J. R.; Vetter, T.W.; Zeisler, R.; Marlow, A.F.; Moreno-Ramirez, M.G. et. al. Microporous and Mesoporous Mater. **2008**,*107*, 252.

S5. Boys, S. F.; Bernardi, F. Mol. Phys. **1970**, *19*, 553.

S6. Bottin, F.; Leroux, S.; Knyazev, A.; Zerah, G. Large-scale Ab Initio Calculations Based on Three Levels of Parallelization. *Comput. Mater. Sci.* **2008**, *42*, 329-336.

S7. Gonze, X.; Amadon, B.; Anglade, P.-M.; Beuken, J.-M.; Bottin, F.; Boulanger, P.; Bruneval, F.; Caliste, D.; Caracas, R.; Cote, M.; Deutsch, T.; Genovese, L.; Ghosez, P.; Giantomassi, M.; Goedecker, S.; Hamann, D. R.; Hermet, P.; Jollet, F.; Jomard, G.; Leroux,

S.; Mancini, M.; Mazevet, S.; Oliveira, M. J. T.; Onida, G.; Pouillon, Y.; Rangel, T.; Rignanese, G.-M.; Sangalli, D.; Shaltaf, R.; Torrent, M.; Verstraete, M. J.; Zerah, G.; Zwanziger, J. W. *Comput. Phys. Commun.* **2009**, *180*, 2582-2615.

S8. Torrent, M.; Jollet, F.; Bottin, F.; Zerah, G.; Gonze, X. Implementation of the Projector Augmented-Wave Method in the ABINIT Code: Application to the Study of Iron under Pressure. *Comput. Mater. Sci.* 2008, *42*, 337-351.

S9. Anisimov, V. I.; Zaanen, J.; Andersen, O. K. Band Theory and Mott Insulators: Hubbard *U* instead of Stoner *I. Phys. Rev. B* 1991, 44, 943-.

S10. Mann, G. W., Lee, K., Cococcioni, M., Smit, B., Neaton, J. B. First-principles Hubbard U approach for small molecule binding in metal-organic Frameworks. J. Chem. Phys. **2016**, 144, 174104.

S11. Živkovic, A., Roldan, A., de Leeuw, N . H., Density functional theory study explaining the underperformance of copper oxides as photovoltaic absorbers. Phys. Rev. B **99 (2019)** 035154.

S12. Grimme, S.; Antony, J.; Ehrlich, S.; Krieg, H. A Consistent and Accurate *Ab Initio* Parametrization of Density Functional Dispersion Correction (DFT-D) for the 94 Elements H-Pu. *J. Chem. Phys*. **2010**, *132*, 154104.